JEM Journal of Experimental Medicine

BRIEF DEFINITIVE REPORT

Bromodomain protein BRD4 directs and sustains CD8 T cell differentiation during infection

J. Justin Milner[1], Clara Toma[1], Sara Quon[1], Kyla Omilusik[1], Nicole E. Scharping[1], Anup Dey[2], Miguel Reina-Campos[1], Hongtuyet Nguyen[1], Adam J. Getzler[3], Huitian Diao[3], Bingfei Yu[1], Arnaud Delpoux[1], Tomomi M. Yoshida[1], Deyao Li[4,5], Jun Qi[4,5], Adam Vincek[6], Stephen M. Hedrick[1,7], Takeshi Egawa[8], Ming-Ming Zhou[6], Shane Crotty[9,10], Keiko Ozato[2], Matthew E. Pipkin[3], and Ananda W. Goldrath[1]

In response to infection, pathogen-specific CD8 T cells differentiate into functionally diverse effector and memory T cell populations critical for resolving disease and providing durable immunity. Through small-molecule inhibition, RNAi studies, and induced genetic deletion, we reveal an essential role for the chromatin modifier and BET family member BRD4 in supporting the differentiation and maintenance of terminally fated effector CD8 T cells during infection. BRD4 bound diverse regulatory regions critical to effector T cell differentiation and controlled transcriptional activity of terminal effector–specific super-enhancers in vivo. Consequentially, induced deletion of *Brd4* or small molecule–mediated BET inhibition impaired maintenance of a terminal effector T cell phenotype. BRD4 was also required for terminal differentiation of CD8 T cells in the tumor microenvironment in murine models, which we show has implications for immunotherapies. Taken together, these data reveal an unappreciated requirement for BRD4 in coordinating activity of cis regulatory elements to control CD8 T cell fate and lineage stability.

Introduction

CD8 T cells are critical mediators of host defense against intracellular pathogens and malignancy (Chang et al., 2014). Upon recognition of cognate antigen, CD8 T cells become activated, rapidly expand, and differentiate into effector cells critical for resolution of disease. Following pathogen clearance, a relatively small population of antigen-specific effector cells persists and gives rise to memory T cells. It is apparent that the CD8 T cell response to infection is accompanied by extensive functional heterogeneity at both the effector and memory phases (Jameson and Masopust, 2018). Understanding the molecular signals controlling T cell differentiation provides insight for harnessing discrete T cell states for therapeutic strategies.

Differential expression levels of KLRG1 and CD127 delineate effector populations with distinct fates during acute infections (Chang et al., 2014; Joshi et al., 2007; Kaech et al., 2003). Nascent cytotoxic effector CD8 T cells rapidly lose expression of CD127—expressed by naive cells—and form a transitional population of CD127^{lo}KLRG1^{lo} early effector cells (EECs) before upregulation of KLRG1 or CD127 (Diao and Pipkin, 2019). KLRG1 expression correlates with terminal differentiation, and CD127 marks cells with a greater degree of memory potential (Chang et al., 2014; Joshi et al., 2007). As such, KLRG1^{lo}CD127^{hi} cells are referred to as memory precursor T cells (MP cells) and KLRG1^{hi}CD127^{lo} cells as terminal effector T cells (TE cells). MP cells display enhanced multipotency compared with TE cells and more efficiently give rise to central memory T cells (T_{CM} cells), effector memory T cells (T_{EM} cells), and tissue-resident memory T cells (T_{RM} cells; Kaech et al., 2003; Mackay et al., 2013; Milner and Goldrath, 2018); however, select TE cells are able to persist for several months after infection, forming a terminally differentiated T_{EM} cell population (t-T_{EM} cells) or long-lived effector population (Kurd et al., 2020; Milner et al., 2020a; Milner et al., 2020b; Olson et al., 2013). Canonical transcription factors known to regulate antiviral T cell differentiation include Id3 (Ji et al., 2011; Yang et al., 2011), TCF1 (Zhou et al., 2010), Bcl6 (Ichii et al., 2002; Liu et al., 2019), STAT3 (Cui et al., 2011), and Foxo1 (Kim

[1]Division of Biological Sciences, University of California San Diego, La Jolla, CA; [2]Division of Developmental Biology, National Institute of Child Health and Human Development, National Institutes of Health, Bethesda, MD; [3]Department of Immunology and Microbiology, The Scripps Research Institute, Jupiter, FL; [4]Department of Cancer Biology, Dana-Farber Cancer Institute, Boston, MA; [5]Department of Medicine, Harvard Medical School, Boston, MA; [6]Department of Pharmacological Sciences, Icahn School of Medicine at Mount Sinai, New York, NY; [7]Department of Cellular and Molecular Medicine, University of California San Diego, La Jolla, CA; [8]Department of Pathology and Immunology, Washington University School of Medicine, St. Louis, MO; [9]Division of Vaccine Discovery, La Jolla Institute for Allergy and Immunology, La Jolla, CA; [10]Division of Infectious Diseases, Department of Medicine, University of California San Diego, La Jolla, CA.

A. Delpoux died on June 30, 2019. Correspondence to Ananda W. Goldrath: agoldrath@ucsd.edu.

et al., 2013; Hess Michelini et al., 2013; Utzschneider et al., 2018) as critical regulators of MP/T_{CM} cells, and Id2 (Cannarile et al., 2006; Knell et al., 2013; Masson et al., 2013), Zeb2 (Dominguez et al., 2015; Omilusik et al., 2015; Omilusik et al., 2018), Blimp1 (Kallies et al., 2009; Rutishauser et al., 2009), STAT4 (Mollo et al., 2014), and T-bet (Joshi et al., 2007) are required for more terminally differentiated populations.

Analogous to infection responses, tumor-infiltrating CD8 T lymphocytes (TILs) also exist in a range of cell states, wherein multipotent progenitor exhausted cells can be distinguished as PD-$1^{Int/hi}$Slamf6^{hi}Tim3^{lo} and express elevated levels of the transcription factors TCF1 and Id3 compared with terminally exhausted cells that are PD-1^{hi}Tim3^{hi} and $Id3^{lo}$TCF1^{lo} (Im et al., 2016; Miller et al., 2019; Milner et al., 2020b; Siddiqui et al., 2019). Progenitor exhausted cells provide sustained antitumor immunity and are more responsive to immunotherapies, such as checkpoint blockade and therapeutic vaccines (Im et al., 2016; Miller et al., 2019; Siddiqui et al., 2019); therefore, understanding the signals promoting and enforcing CD8 T cell differentiation is relevant for cancer immunotherapies.

Here, we sought to identify transcriptional and epigenetic signals regulating CD8 T cell differentiation over the course of infection. We employed a targeted in vivo RNAi loss-of-function screen to identify transcription factors and epigenetic regulators controlling the differentiation of CD8 T cells during acute viral infection. The pooled screening approach identified an essential role for the chromatin modifier bromodomain-containing protein 4 (BRD4) in regulating T cell fate specification, and through multiple distinct approaches, we show that BRD4 is required for both promoting and sustaining a terminally differentiated CD8 T cell state. Through genome-wide binding analysis, we found that BRD4 binds near genes critical to CD8 T cell differentiation and effector subset identity. Remarkably, >99% of TE cell super-enhancers were occupied by BRD4 in vivo, and consequentially, induced deletion of *Brd4* resulted in loss of super-enhancer transcriptional activity and impaired maintenance of a TE phenotype. Last, we extended our findings to the tumor microenvironment, where we demonstrated that BRD4 supports formation of terminally differentiated CD8 T cells in tumors, and therapeutic targeting of BRD4 in CD8 T cells can modify immunotherapy efficacy. Taken together, we define an essential role for BRD4 in linking cis regulatory elements to CD8 T cell differentiation and function. Understanding how effector and memory CD8 T cell subset differentiation can be manipulated in vivo, such as targeting of bromodomain-containing proteins with small-molecule inhibitors, holds promise for vaccination or immunotherapy approaches designed for controlling infection and malignancy.

Results and discussion

In vivo loss-of-function screen reveals chromatin modifier BRD4 as a critical regulator of CD8 T cell differentiation during infection

Chromatin modifiers and transcription factors can differentially regulate the formation of divergent cell states without varying expression levels, often limiting our ability to predict how key regulators of gene expression control T cell lineage specification (Milner et al., 2017; Yu et al., 2017). We have previously used a pooled in vivo RNAi screening strategy (Chen et al., 2014) to identify functional regulators of T_{RM} cell formation (Milner et al., 2017). Using a similar microRNA-based shRNA (shRNAmir) library and approach (Chen et al., 2014; Milner et al., 2017), we screened 215 shRNAmirs to identify functional regulators of early memory T cell differentiation during lymphocytic choriomeningitis virus (LCMV) infection (Fig. 1 A and Fig. S1 A). Several transcription factors known to be important for long-lived memory or T_{CM} cells were confirmed in this screening approach, including Id3 (Ji et al., 2011; Yang et al., 2011), Klf2 (Bai et al., 2007; Hart et al., 2012; Preston et al., 2013), and Bcl6 (Ichii et al., 2002; Liu et al., 2019), whereas Id2 (Cannarile et al., 2006; Knell et al., 2013; Masson et al., 2013) and Runx3 (Wang et al., 2018) were required for formation of $CD62L^{lo}$ t-T_{EM}/T_{EM} cells relative to T_{CM} cells (Fig. 1 A and Table S1). A notable hit from this loss-of-function screen included chromatin modifier BRD4. *Brd4* shRNAmirs were enriched in the $CD62L^{hi}$ population relative to $CD62L^{lo}$ cells, identifying BRD4 as a putative mediator of t-T_{EM}/T_{EM} cell differentiation. BRD4 has emerged as a key regulator of cellular differentiation in multiple contexts, including diverse cancer types (Donati et al., 2018; Filippakopoulos et al., 2010; Ren et al., 2018), hematopoietic stem cells (Dey et al., 2019), CD4 T cell populations (Bandukwala et al., 2012; Cheung et al., 2017a; Cheung et al., 2017b; Mele et al., 2013), and CD8 T cells in vitro (Chee et al., 2020; Georgiev et al., 2019; Kagoya et al., 2016), but the role of BRD4 in regulating T cell differentiation in vivo and in the context of infection remains unclear.

BRD4 is a member of the BET protein family, functioning in many cases as a chromatin reader that binds acetylated lysine residues in enhancer regions and establishes a molecular scaffold for controlled transcription of critical genes (Dey et al., 2019; Lee et al., 2017; Lovén et al., 2013). We first sought to validate BRD4 as a putative positive regulator of TE cell and/or early t-T_{EM} cell formation as observed in the in vivo screen. Two distinct *Brd4* shRNAmirs mediated 70%–80% knockdown efficiency, confirming their on-target activity (Fig. S1 B). Congenically distinct CD8 T cells expressing a transgenic TCR recognizing the LCMV GP_{33-41} epitope presented by MHCI (P14 cells) were transduced with a control retrovirus—encoding *Cd19* shRNAmir—or a *Brd4* shRNAmir encoding retrovirus and transferred into recipient mice subsequently infected with LCMV. Consistent with the loss-of-function screen results, we found that *Brd4* RNAi impaired the formation of $CD127^{lo}CD62L^{lo}$ t-T_{EM} cells, resulting in a greater frequency of T_{CM} cells (Fig. 1 B). We also assessed how depletion of BRD4 impacted CD8 T cell differentiation over the course of LCMV infection and detected a reduced frequency of $KLRG1^{hi}$ P14 cells at all time points, as well as an increased frequency of $CD127^{lo}KLRG1^{lo}$ EECs on day 5 of infection (Fig. 1 C). CX3CR1 expression levels on CD8 T cells are reflective of the degree of terminal differentiation (Böttcher et al., 2015; Gerlach et al., 2016; Milner et al., 2020a), and knockdown of *Brd4* resulted in a reduced frequency of $CX3CR1^{hi}$ P14 cells (Fig. 1 D). Taken together, informed through a pooled in vivo screening approach, we identified an essential role for BRD4 in the formation of TE cells as well as the more terminally

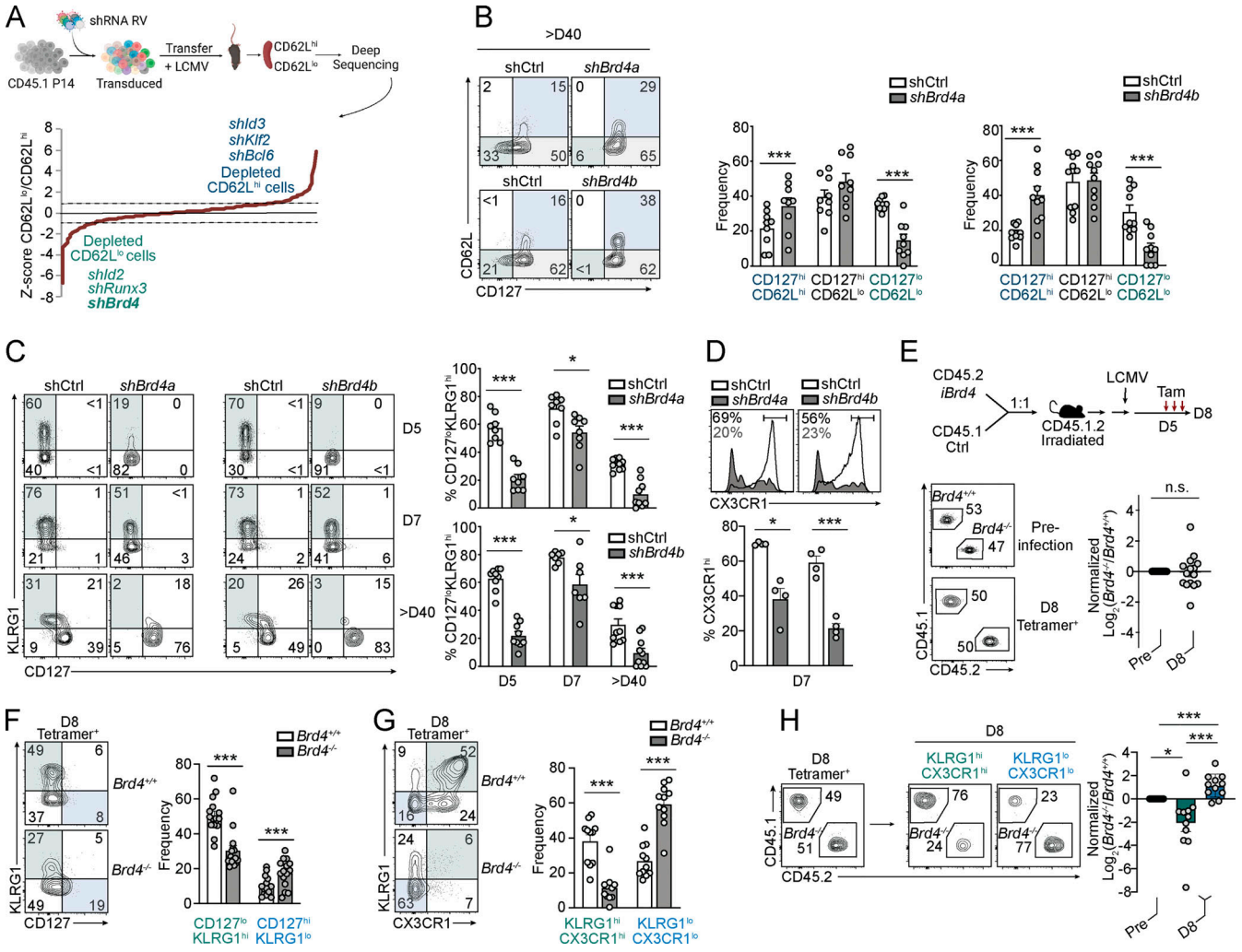

Figure 1. **In vivo RNAi screen reveals BRD4 as a critical regulator of CD8 T cell differentiation during infection. (A)** Relative enrichment of shRNAmirs in splenic CD62L^{hi} and CD62L^{lo} cells from an in vivo RNAi screen, reported as the average Z-score from three independent screens where each independent screen was performed by pooling DNA from sorted P14 populations from 15–18 mice. **(B–D)** Congenically distinct P14 cells were transduced with *Brd4* shRNA–encoding or control shRNA–encoding retroviruses and transferred into recipient mice subsequently infected with LCMV. Frequency of T_{CM}, T_{EM}, t-T_{EM} memory T cell populations (B), frequency of CD127^{lo}KLRG1^{hi} expressing cells (C), or frequency of CX3CR1^{hi} cells in response to LCMV infection (D). **(E)** Bone marrow chimera mice were generated by adoptive transfer of 1:1 mixed bone marrow cells from CD45.1 *Brd4*$^{+/+}$ control mice (Ctrl) and CD45.2 *Brd4*$^{fl/fl}$*Ert2*$^{Cre/+}$ mice (inducible *Brd4* [*iBrd4*]) into irradiated mice (left). Reconstituted mice were infected with LCMV and treated with tamoxifen on days 5–7 of infection to induce deletion of *Brd4*. Representative flow cytometry plots (left) and quantification (right) of the ratio of *Brd4*$^{fl/fl}$*Ert2*$^{Cre/+}$ CD8 T cells and control cells before infection and 8 d after infection. **(F and G)** Frequency of CD127 and KLRG1 (F) or CX3CR1 and KLRG1 expressing tetramer$^+$ cells from E (G). **(H)** Representative flow cytometry plots indicating the ratio of *Brd4*$^{fl/fl}$*Ert2*$^{Cre/+}$ and control tetramer$^+$ CD8 T cells (left, similar to E) and the ratio of *Brd4*$^{fl/fl}$*Ert2*$^{Cre/+}$ and control cells among all tetramer$^+$ KLRG1^{hi}CX3CR1^{hi} and KLRG1^{lo}CX3CR1^{lo} CD8 T cell populations (right). Graphs show mean ± SEM of n = 7–10 mice pooled from two or three independent experiments (B and C); n = 4 from one representative of two independent experiments at days 5 or 7 of infection (D); n = 15 pooled from three independent experiments (E and F) or n = 11 pooled from two independent experiments (G and H). *, P < 0.05; ***, P < 0.005. Symbols represent an individual mouse (B–H).

fated memory population (i.e., CD127^{lo}CD62L^{lo}) t-T_{EM} cells. Additionally, we previously detected BRD4 as a top candidate in a T_{RM} cell differentiation screen (Milner et al., 2017), and consistent with these findings, *Brd4* RNAi impaired the early formation of CD69^{hi}CD103^{hi} cells in the intestinal epithelium (Fig. S1 C).

We next generated mixed bone marrow chimeric mice comprised of a 1:1 mixture of congenically distinct *Brd4*$^{fl/fl}$*Ert2*$^{Cre/+}$ bone marrow and *Brd4*$^{+/+}$ bone marrow to further evaluate a CD8 T cell–intrinsic role for BRD4 and validate shRNAmir knockdown studies (Fig. 1 E). Reconstituted chimeric mice were infected with LCMV and tamoxifen was administered on days 5–7 of infection to induce Cre-mediated deletion of *Brd4*. Induced depletion of BRD4 on days 5–7 of infection did not impact the overall number of tetramer$^+$ *Brd4*$^{fl/fl}$*Ert2*$^{Cre/+}$ cells as the mean ratio of BRD4-deficient, and control cells remained at a similar 1:1 ratio on day 8 of infection (Fig. 1 E and Fig. S1 D); however, deletion of *Brd4* resulted in a reduction in the frequency of antigen-specific, terminally fated KLRG1^{hi}CD127^{lo} TE cells and a greater proportion of KLRG1^{lo}CD127^{hi} MP cells

(Fig. 1 F). Loss of BRD4 also resulted in a dramatically reduced frequency of KLRG1^{hi}CX3CR1^{hi} cells and a greater frequency of KLRG1^{lo}CX3CR1^{lo} cells (Fig. 1 G). Despite no change in the overall mean ratio of total WT control and mutant GP_{33-41}–specific cells on day 8 of infection (Fig. 1 E), we detected a greater abundance of KLRG1^{lo}CX3CR1^{lo} cells with loss of BRD4 and a decreased overall abundance of KLRG1^{hi}CX3CR1^{hi} cells (Fig. 1 H). Further highlighting the critical and dynamic role of BRD4 in CD8 T cell immunity, we found that deletion of *Brd4* at early infection time points—days 1–5 of infection—not only impacts cellular differentiation (as in Fig. 1 F) but also affects the overall accumulation of antigen-specific CD8 T cells (Fig. S1, E and F). Therefore, BRD4 is a critical mediator of CD8 T cell differentiation during acute viral infection and is required for optimal formation of a terminally differentiated cell state.

In vivo BET inhibition impairs CD8 T cell differentiation during viral infection

BET proteins bear characteristic tandem bromodomains (BDs; BD1 and BD2) that bind acetylated lysine residues facilitating protein–protein interactions (Shi and Vakoc, 2014). Widely used BET inhibitors JQ1 and OTX-015 potently impair the activity of BET proteins, especially BRD4, through competitively binding bromodomains (Boi et al., 2015; Filippakopoulos et al., 2010). Additionally, the small molecule MS402 selectively targets BD1 of BRD4, preferentially inhibiting BRD4-induced expression of genes key to lineage specification (Cheung et al., 2017a). BET protein inhibitors represent promising therapeutic modalities for a number of disease states ranging from cancer to autoimmunity. In vitro treatment with BET inhibitors has been shown to modulate T cell activation (Chee et al., 2020; Georgiev et al., 2019; Kagoya et al., 2016); however, the in vivo effects of BET inhibition and small-molecule targeting of BRD4 in CD8 T cell differentiation during infection is not known.

Given the striking impact of BRD4 deficiency on TE cell differentiation, we tested if this phenotype could be recapitulated through BET inhibition in vivo. P14 cells were adoptively transferred to recipient mice subsequently infected with LCMV and treated with JQ1, MS402, OTX-O15, or corresponding vehicle controls from days 1–4 of infection (Fig. 2 A). On day 5 of infection, we assessed the phenotype of donor P14 cells and found that all BET inhibitors impaired the early formation of KLRG1^{hi} TE cells, resulting in a greater proportion of KLRG1^{lo} EECs (Fig. 2 A), consistent with RNAi and genetic deletion studies. Failure to optimally generate KLRG1^{hi} cells was also reflected by reduced frequencies of CX3CR1^{hi}, CD43^{lo}, and CD27^{lo} cells, but an elevated frequency of CD62L^{hi} cells (Fig. 2 B). Additionally, JQ1 treatment impaired the early formation of intestinal CD69^{hi}CD103^{hi} T_{RM} cells (Fig. S1 G), consistent with RNAi studies (Fig. S1 C). As there are four members of the BET protein family (BRDT, BRD2, BRD3, and BRD4), it was unclear what degree the observed phenotype of BET inhibition was solely due to BRD4 inhibition. Only robust expression of *Brd2* and *Brd4* was detected in CD8 T cell populations during LCMV infection (Fig. S2 A), with minimal variation in expression between CD8 T cell subsets. To clarify the effect of BET inhibitors on CD8 T cell fate, we evaluated a regulatory role for BRD2 using two distinct *Brd2* shRNAmirs that result in ∼60% to 70% *Brd2* knockdown efficiency (Fig. S2 B). *Brd2* RNAi resulted in a subtle loss of KLRG1^{hi} cells on day 5 (Fig. 2 C) and day 7 of infection (Fig. S2 C); therefore, we concluded that, while both *Brd2* and *Brd4* regulated aspects of CD8 T cell differentiation, loss of BRD4 activity likely conferred the strongest BET-mediated contribution to impaired differentiation of TE cells during LCMV infection. Furthermore, BET proteins are broadly expressed in a wide range of cell types, and thus, indirect effects of BET inhibition on other cell types may also contribute to the observed phenotype in virus-specific CD8 T cells.

To further evaluate the degree to which BET inhibition impairs BRD4 activity in CD8 T cells in vivo, we profiled the transcriptome of KLRG1^{lo}CD127^{lo} EEC P14 cells from JQ1- or vehicle-treated mice as well as sh*Brd4* or shCtrl P14 cells in a mixed transfer setting (Fig. 2 D). Splenic KLRG1^{lo}CD127^{lo} EECs were sorted for RNA sequencing analyses rather than bulk P14 cells to avoid confounding transcriptional changes caused by differing frequencies of TE cells, as well as to further understand the perceived impairment in the transition from an EEC state to a TE state in BRD4 knockdown cells (Fig. 1 C and Fig. 2 A). We found that 89% of the transcripts downregulated by *Brd4* RNAi were also suppressed by in vivo JQ1 treatment, and nearly 80% of transcripts upregulated by *Brd4* RNAi were similarly upregulated by JQ1 treatment (Fig. 2 D). Gene set enrichment analysis (Fig. 2 D) further confirmed that JQ1-mediated BET inhibition and *Brd4* knockdown exerted similar transcriptional changes in KLRG1^{lo} EEC P14 cells at early times after LCMV infection. Validation of key differentially expressed genes revealed elevated TCF1 (encoded by *Tcf7*) and Eomes, reduced GzB production, but similar expression of T-bet, consistent with mRNA levels for these targets (Fig. 2, E and F). These data suggest that BET inhibition might represent a therapeutic opportunity for targeting BRD4 activity and modulating CD8 T cell differentiation in vivo.

BRD4 binds fate-specifying genes to coordinate effector CD8 T cell differentiation

Early inhibition of BRD4 activity with JQ1 or depletion of BRD4 through shRNAmir approaches limited the differentiation of terminally fated effector CD8 T cells, resulting in a greater frequency of the more multipotent EEC population (Fig. 2). Furthermore, induced *Brd4* deletion resulted in a reduced abundance of terminally differentiated cells and enhanced accumulation of memory-like KLRG1^{lo}CX3CR1^{lo} tetramer^{+} cells (Fig. 1 H). These findings indicate that BRD4 is important for TE cell differentiation and may facilitate maintenance of the TE cell population. To further address this, we profiled the transcriptome of TE, EEC, and MP tetramer^{+} cells following induced deletion of *Brd4* on days 5–7 of LCMV infection sorted from mixed bone marrow chimera mice (Fig. 3 A). Loss of *Brd4* dramatically changed the gene-expression program in all three effector populations. Principle component analysis revealed that *Brd4*-deficient populations were transcriptionally distinct from control populations (Fig. 3 A); however, comparison of expression levels of TE-, EEC-, and MP-signature gene sets between control versus mutant subsets revealed that BRD4 was required for expression of lineage-specific genes in each cell type, as TE,

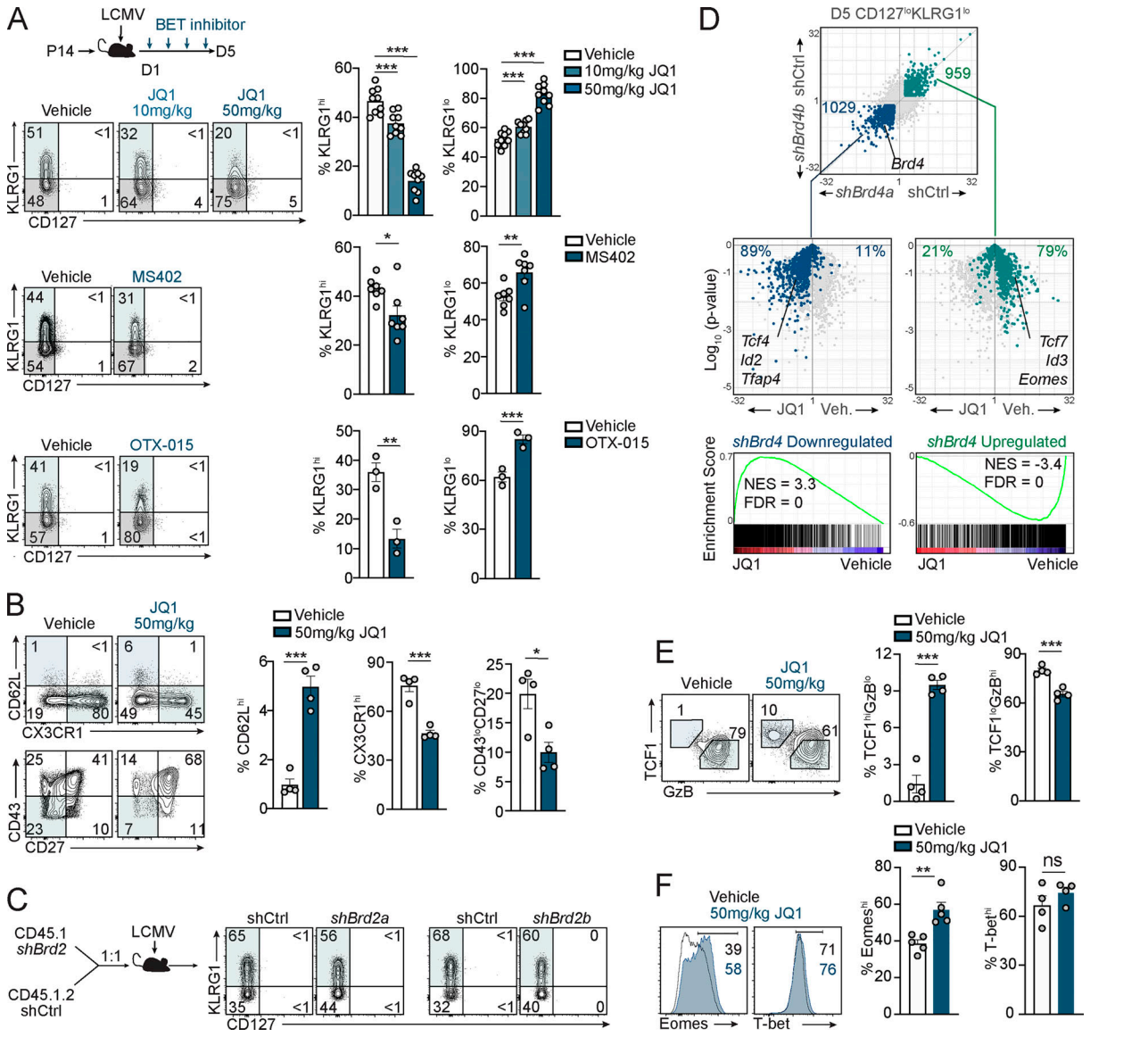

Figure 2. **In vivo BET inhibition impairs CD8 T cell differentiation during infection.** P14 CD8 T cells were transferred into congenically distinct recipient mice subsequently infected with LCMV. **(A)** Infected mice were treated with 50 mg/kg JQ1, 10 mg/kg JQ1, 40 mg/kg MS402, 50 mg/kg OTX-015, or corresponding vehicle controls. Frequency of splenic KLRG1^{hi} and KLRG1^{lo} cells on day 5 of infection. **(B)** Frequency of CD62L^{hi}, CX3CR1^{hi}, and CD43^{lo}CD27^{lo} cells following daily 50 mg/kg JQ1 or vehicle treatments on day 7 of infection. **(C)** Congenically distinct P14 cells were transduced with *Brd2* shRNA– or control shRNA–encoding retroviruses and transferred into recipient mice subsequently infected with LCMV. Representative flow cytometry plots (right) indicate the frequency of KLRG1^{hi}CD127^{lo}-expressing cells on day 5 of infection. **(D)** On day 5 of infection, CD127^{lo}KLRG1^{lo} EECs were sorted for RNA sequencing analysis following the experimental schematic outlined in A or in a mixed transfer setting for each shRNAmir targeting *Brd4*. Expression of genes co-downregulated (blue, ≥1.3-fold) or co-upregulated (green, ≤1.3-fold) in BRD4-deficient cells (top) was evaluated in P14 cells sorted from JQ1 or vehicle-treated mice (middle) and corresponding gene set enrichment analyses were performed (bottom). **(E)** Frequency of TCF1^{hi} or GzB^{hi} P14 cells following daily 50 mg/kg JQ1 or vehicle treatments on day 7 of infection. **(F)** T-box transcription factor expression in P14 cells following daily 50 mg/kg JQ1 or vehicle treatments on day 7 of infection. Graphs show mean ± SEM of *n* = 9 mice pooled from three independent experiments (A, top); *n* = 7 pooled from two independent experiments (A, middle); *n* = 4 from one representative of two independent experiments at days 5 or 7 of infection (A, bottom); *n* = 4–5 from one representative of two independent experiments on day 7 of infection (B, E, and F); and *n* = 4 from one representative of two independent experiments on day 5 of infection (C). RNA sequencing was performed in duplicate, wherein each replicate consisted of KLRG1^{lo}CD127^{lo} sorted P14 cells pooled from two mice on day 5 of LCMV infection. *, P < 0.05; **, P < 0.01; ***, P < 0.005. NES, normalized enrichment score; FDR, false discovery rate q value. Symbols represent an individual mouse (A–C, E, and F).

EEC, and MP signature transcripts were predominantly downregulated in each BRD4-deficient subset compared with the corresponding WT subset (Fig. 3 B). This finding was further exemplified through volcano plots (Fig. 3 C, top) and gene set enrichment analyses (Fig. 3 C, bottom), wherein BRD4-deficient effector T cells failed to upregulate 62%–82% of the lineage-specific gene program. Notably, BRD4-deficient TE cells were enriched for MP and EEC gene expression signatures relative to control TE cells, demonstrating that induced loss of BRD4 resulted in enhanced expression of genes associated with less terminally fated T cell states (Fig. 3 D). Taken together, these data indicate that BRD4 was critical for promoting and/or

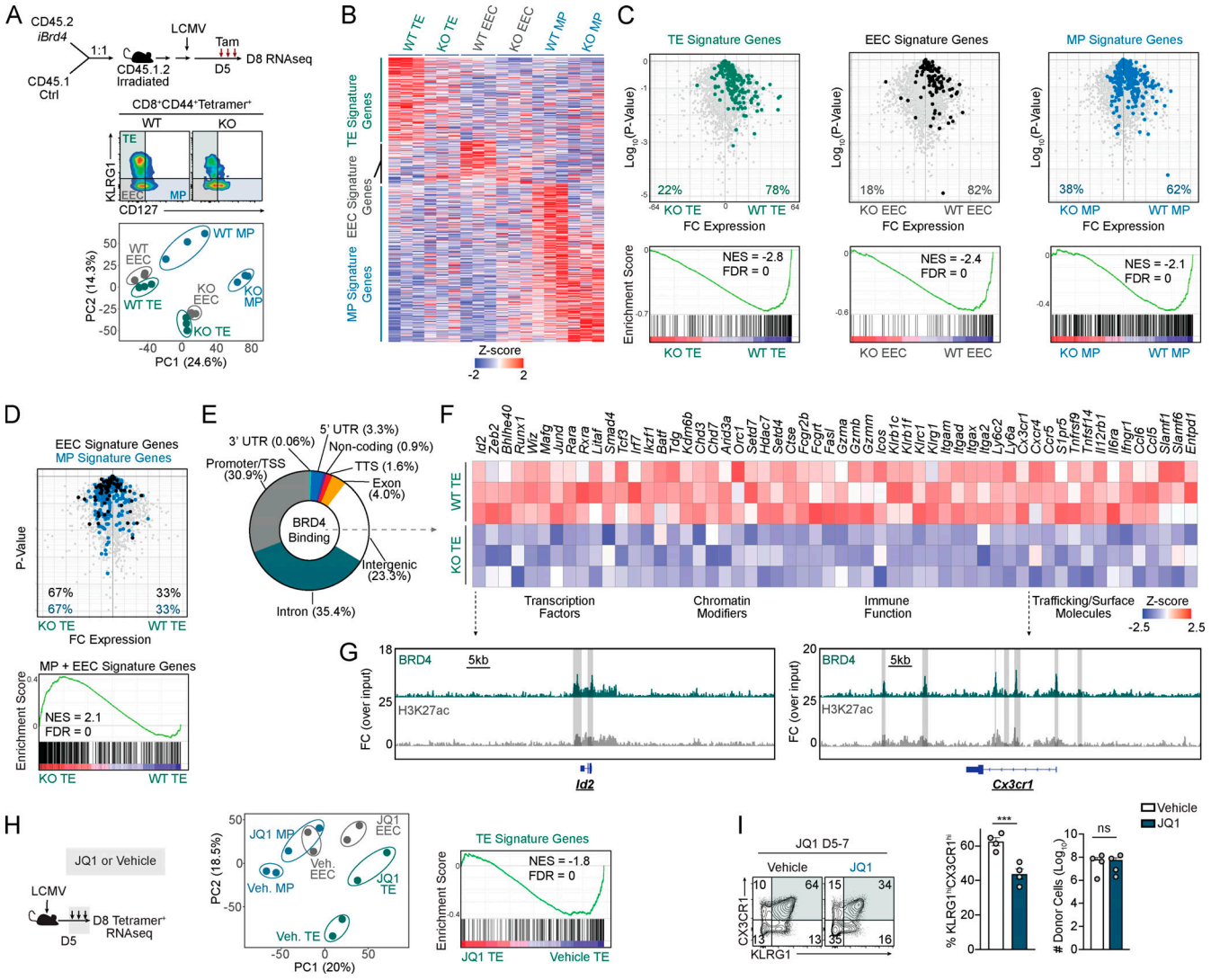

Figure 3. **BRD4 binds fate-specifying genes to coordinate effector CD8 T cell differentiation. (A)** Reconstituted mixed bone marrow chimera mice were infected with LCMV and treated with tamoxifen on days 5–7 of infection. On day 8 of infection, tetramer$^+$ CD127^{hi}KLRG1^{lo} MP, CD127^{lo}KLRG1^{lo} EEC, and CD127^{lo}KLRG1^{hi} TE cells were sorted for RNA sequencing analysis, and principal component analysis of transcriptomic data was performed (bottom). RNA sequencing analysis was performed in triplicate, wherein each sample was composed of cells pooled from two mice. **(B)** Gene expression profile of TE, EEC, and MP signature gene sets in sorted *Brd4*$^{+/+}$ WT and *Brd4*$^{-/-}$ KO populations from experimental setup in A. **(C)** Volcano plots (top) and gene set enrichment analyses (bottom) of signature TE, EEC, and MP gene sets between *Brd4*$^{+/+}$ WT and *Brd4*$^{-/-}$ KO populations from A. **(D)** Volcano plots (top) and gene set enrichment analyses (bottom) of signature EEC and MP gene sets between *Brd4*$^{+/+}$ WT TE and *Brd4*$^{-/-}$ KO TE populations. **(E)** Distribution of genome-wide BRD4 binding in TE P14 cells sorted on day 8 of LCMV infection. ChIP-seq analysis was performed in duplicate, wherein each sample was composed of cells pooled from five mice. **(F)** Expression profile of genes relevant to CD8 T cell differentiation, migration, and function in WT and KO TE cells occupied by BRD4 in TE cells in vivo. **(G)** Representative BRD4 and H3K27ac peaks near *Id2* and *Cx3cr1* loci in TE cells with reproducible peaks highlighted (gray) using the ENCODE ChIP-seq pipeline. **(H)** Following LCMV infection, mice were treated with 50 mg/kg JQ1 or vehicle on days 5–7 of infection, and tetramer$^+$ cells were sorted for RNA sequencing analysis, and subsequent principal component analysis (middle) or gene set enrichment analysis with TE signature genes (right) was performed. Samples were sorted in duplicate, wherein each sample was combined from two mice. **(I)** Donor P14 cells were phenotyped for CX3CR1 and KLRG1 expression levels on day 8 of LCMV infection following JQ1 or vehicle treatment on days 5–7. Graphs show mean ± SEM of $n = 4$ mice from one representative of two independent experiments (I). ***, $P < 0.005$. NES, normalized enrichment score; FDR, false discovery rate q value; TSS, transcription start site; TTS, transcription termination site; UTR, untranslated region. Symbols represent an individual mouse (I).

maintaining the identity of each of the specialized effector CD8 T cell populations (i.e., TE, EEC, and MP) during acute infection, especially TE cells (Fig. 3, C and D).

In diverse cell types, BET proteins coordinate expression of fate-determining molecules primarily through recruitment of transcriptional and chromatin-modifying complexes to regulatory enhancer regions (Cochran et al., 2019; Shi and Vakoc, 2014). Given that induced deletion of *Brd4* resulted in an impairment in TE cell formation as well as a loss of TE cell transcriptional identity, we speculated that BRD4 binds to and promotes expression of key genes essential to effector T cell differentiation and the TE lineage. Genome-wide BRD4 binding was profiled in splenic P14 TE cells on day 8 of LCMV infection using chromatin immunoprecipitation sequencing (ChIP-seq).

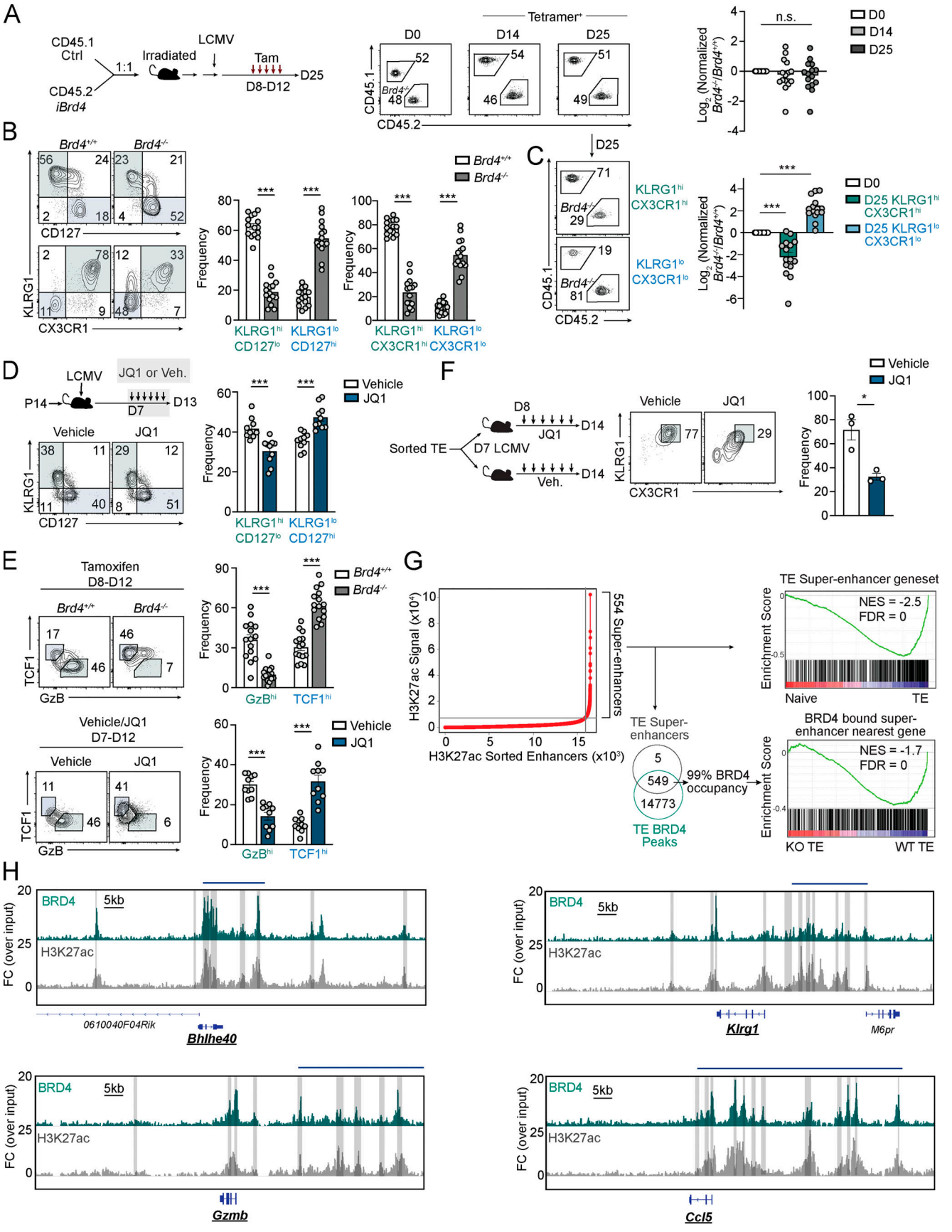

Figure 4. **BRD4 enforces effector identity and regulates transcriptional activity of TE super-enhancers. (A)** Reconstituted mixed bone marrow chimeric mice were infected with LCMV and subsequently treated with tamoxifen daily on days 8–12 of infection (left). Frequency of tetramer⁺ *Brd4*$^{-/-}$ KO and *Brd4*$^{+/+}$

WT cells in peripheral blood (right). **(B)** Frequency of CD127, KLRG1, and CX3CR1 expressing tetramer$^+$ cells on day 25 of infection from experimental setup in A. **(C)** Ratio of *Brd4$^{fl/fl}$ Ert2$^{Cre/+}$* and control cells among all KLRG1^{hi}CXCR1^{hi} or KLRG1^{lo}CX3CR1^{lo} tetramer$^+$ CD8 T cell populations from A. **(D)** Naive P14 cells were transferred to congenically distinct recipient mice and subsequently infected with LCMV. Recipient mice were treated with 50 mg/kg JQ1 or vehicle daily from days 7–12 of infection. On day 13 of infection, the frequency of CD127- and KLRG1-expressing P14 cells was evaluated. **(E)** Frequency of TCF1- and GzB-expressing cells from experimental setup in A or D. **(F)** Sorted KLRG1^{hi} P14 cells were transferred to infection-matched recipient mice that were subsequently treated with daily 50 mg/kg JQ1 or vehicle (left). Frequency of KLRG1- and CX3CR1-expressing donor P14 cells on day 14 of infection. **(G)** ROSE algorithm identified super-enhancers from ENCODE pipeline–processed H3K27ac ChIP-seq data from sorted TE cells (left; Yu et al., 2017). Gene set enrichment analysis of genes nearest to TE super-enhancers compared between naive P14 cells and TE P14 cells (top right). Overlap of TE super-enhancers and TE BRD4 peaks (bottom left), and gene set enrichment analysis of expression levels of nearest genes of BRD4 bound super-enhancers compared between tetramer$^+$ *Brd4$^{-/-}$* KO TE and tetramer$^+$ *Brd4$^{+/+}$* WT TE (bottom right). **(H)** Representative TE H3K27ac and BRD4 peaks at *Bhlhe40*, *Klrg1*, *Gzmb*, and *Ccl5* loci with reproducible BRD4 peaks highlighted (gray) using the ENCODE ChIP-seq pipeline. Super-enhancer regions are demarcated with a blue line above the tracks. Graphs show mean ± SEM of n = 10–15 mice pooled from three independent experiments (A–E) or n = 3 from one representative experiment (F). *, P < 0.05; ***, P < 0.005. NES, normalized enrichment score; FDR, false discovery rate q value. Symbols represent an individual mouse (A–E).

We detected BRD4 enrichment in gene bodies (comprising only ∼1% to 2% of the genome), with 75.8% of BRD4 peaks located in promoter/transcription start sites, introns, untranslated regions, and transcription termination sites (Fig. 3 E). Examination of key loci bound by BRD4 revealed numerous molecules critical to effector CD8 T cell fate, function, and localization, and many of these relevant BRD4 targets exhibited failed upregulation with BRD4 deficiency (Fig. 3 F). Notable BRD4-sensitive targets included *Id2*, a transcriptional regulator essential for TE cell formation, and chemokine receptor *Cx3cr1*, which is markedly upregulated in TE cells (Fig. 3 F; Böttcher et al., 2015; Cannarile et al., 2006; Gerlach et al., 2016; Omilusik et al., 2018). BRD4 binding was observed at the *Id2* and *Cx3cr1* loci, including near promoter regions (Fig. 3 G). As a key function of BRD4 in other cell types is binding to enhancer regions to promote gene expression (Dey et al., 2019; Lee et al., 2017; Lovén et al., 2013), BRD4 binding patterns were contextualized with H3K27ac marks in TE cells (Yu et al., 2017). Indeed, we identified extensive overlap between BRD4 peaks and H3K27ac peaks (Fig. 3 G); however, the abundance of BRD4 at gene bodies suggests that an additional key role of BRD4 in CD8 T cells is direct transcription of genes in addition to regulating transcriptional activity of enhancers. Certain genes were upregulated with loss of *Brd4*, and this could be attributed to failed upregulation of transcriptional repressors or alternative functions of BRD4 acting to repress select gene targets. In complementary experiments, later chemical inhibition of BRD4 on days 5–7 of infection also dramatically modified the gene expression program in TE, EEC, and MP cell populations compared with cells sorted from vehicle-treated mice (Fig. 3 H). TE cells sorted from mice treated with JQ1 exhibited impaired expression of characteristic TE cell transcripts, as determined through gene set enrichment analysis (Fig. 3 H), and resulted in rapid alterations in the phenotype of antigen-specific CD8 T cells (Fig. 3 I). Taken together, BRD4 binds to and promotes expression of genes central to CD8 T cell differentiation.

BRD4 enforces effector identity and regulates activity of TE super-enhancers

The robust occupancy of BRD4 at critical loci and the reduced expression of key TE cell–specific transcripts in BRD4-deficient cells foreshadowed an essential role for BRD4 in sequentially maintaining TE cell identity in addition to regulating differentiation. We sought to further clarify the role of BRD4 in supporting the maintenance of terminally differentiated effector cells following the peak of infection, after which the TE cell population is relatively stable (Chang et al., 2014). We induced *Brd4* deletion in mixed bone marrow chimeric mice through tamoxifen administration on days 8–12 of infection (Fig. 4 A). Consistent with tamoxifen treatment on days 5–7 of infection, we detected no change in the overall accumulation of *Brd4$^{-/-}$* tetramer$^+$ cells on day 14 or later infection time points (Fig. 4 A); however, despite no change in the accumulation of antigen-specific CD8 cells, induced deletion of *Brd4* resulted in a profound loss in the frequency of CD127^{lo}KLRG1^{hi} and KLRG1^{hi}CX3CR1^{hi} cells and a greater frequency of CD127^{hi}KLRG1^{lo} and KLRG1^{lo}CX3CR1^{lo} cells (Fig. 4 B). Consistent with a role in supporting the maintenance and identity of terminally fated CD8 T cells, we found a reduced accumulation of KLRG1^{hi}CX3CR1^{hi} cells on day 25 of infection, with induced deletion of *Brd4* and an enhanced abundance of multipotent KLRG1^{lo}CX3CR1^{lo} cells (Fig. 4 C). These data indicate that induced deletion of *Brd4* in TE cells resulted in a loss of TE identity, permitting transition to a KLRG1^{lo}CX3CR1^{lo} memory-like phenotype; however, it is also possible that induced deletion of *Brd4* results in the transition of EECs to KLRG1^{lo}CX3CR1^{lo} cells.

We next assessed if delayed BET inhibition paralleled findings from delayed *Brd4* deletion. On days 7–12 of LCMV infection, mice were treated with JQ1 or vehicle (Fig. 4 D). Consistent with delayed deletion experiments, we found that BET inhibition resulted in a reduced frequency of TE cells (Fig. 4 D). Delayed treatment of JQ1 or tamoxifen also resulted in reduced GzB expression and a greater frequency of TCF1^{hi} cells (Fig. 4 E). Finally, to clarify the lineage-specific role of BRD4 in maintaining TE identity, we sorted TE P14 cells, transferred the congenically distinct TE cells into infection-matched recipient mice, and subsequently treated recipients with JQ1 or vehicle from day 8 through day 13 of infection. On day 14 of infection, we evaluated the terminal phenotype of donor cells and found that BET inhibition resulted in a rapid loss of KLRG1 and CX3CR1 expression compared with vehicle-treated mice (Fig. 4 F); therefore, BRD4 is critical in enforcing a terminally differentiated state in TE cells.

Assessment of genome-wide occupancy of BRD4 revealed robust binding in a multitude of lineage-specifying genes critical to the identity of TE cells (Fig. 3 F). In other cell types, super-enhancers (i.e., large clusters of conventional enhancers) are known to control cell identity and can be regulated and

interpreted by BRD4 (Dey et al., 2019; Lee et al., 2017; Lovén et al., 2013); however, the regulation of super-enhancer activity in CD8 T cells remains unexplored. We next sought to understand if BRD4 occupied and regulated super-enhancer regions, potentially explaining the critical role of BRD4 in enforcing TE identity. Similar to previous reports (He et al., 2016), we called 554 TE super-enhancers through the ROSE algorithm using H3K27ac ChIP-seq data of sorted TE cells (Yu et al., 2017), which was processed by the ENCODE ChIP-seq pipeline (Fig. 4 G). Genes nearest to identified super-enhancer regions were characteristically upregulated in TE cells compared with naive cells, supporting the biological relevance and overall robustness of the super-enhancer peak calling (Fig. 4 G, top). Next, we evaluated the extent to which BRD4 occupied these identified super-enhancer regions and found that, remarkably, 549 of 554 (>99%) super-enhancers overlapped with BRD4 binding (Fig. 4 G, bottom). We detected impaired expression of genes associated with BRD4-occupied super-enhancers in BRD4-deficient TE cells (Fig. 4 G, bottom right). Notable super-enhancer regions occupied by BRD4 with failed upregulation of the nearest genes in *Brd4*$^{-/-}$ TE cells included TE-associated genes *Zeb2*, *Gzma*, *Kdm6b*, as well as *Bhlhe40*, *Gzmb*, *Klrg1*, and *Ccl5*, highlighted in Fig. 4 H, implicating BRD4 as a robust regulator of the TE gene expression program.

BRD4 regulates CD8 T cell differentiation in response to tumors

Analogous to CD8 T cell subsets responding to infection, TILs display a range of multipotent to terminally fated states within the tumor microenvironment (Fig. S1 A; Kallies et al., 2020). Given that BRD4 was central to the initiation and maintenance of a terminally differentiated state during infection, we next assessed the role of BRD4 in supporting the differentiation of terminally exhausted cells, characteristically marked by elevated Tim3 expression (Kallies et al., 2020; Miller et al., 2019; Siddiqui et al., 2019), in a mouse model of melanoma. BRD4 was required for the formation of terminally exhausted cells in an antigen-specific CD8 T cell–intrinsic manner, evidenced by a reduced frequency of Tim3^{hi} TILs with *Brd4* knockdown using two distinct shRNAmirs (Fig. 5 A and Fig. S3 A). Consistent with these results, we also found that daily in vivo treatment with JQ1 impaired the formation of Tim3^{hi} tumor-specific TILs (Fig. 5 B). Impaired generation of Tim3^{hi} terminally fated TILs with *Brd4* RNAi or JQ1 treatment emphasizes the central role of BRD4 in coordinating the expression of genes critical to terminal CD8 T cell differentiation (as in Fig. 3 F and Fig. 4 H), and this fate-specifying activity is further underscored by a BRD4-occupied super-enhancer region near *Havcr2* encoding Tim3 (Fig. 5 C).

BET inhibition is an emerging treatment for diverse malignancies and is currently under investigation in >25 clinical trials (Khandekar and Tiriveedhi, 2020); however, the focus of BET inhibition in cancer therapies has been predominantly limited to direct effects on malignant cells (Boi et al., 2015; Delmore et al., 2011; Filippakopoulos et al., 2010; Khandekar and Tiriveedhi, 2020; Ott et al., 2012; Shi and Vakoc, 2014; Shu et al., 2016), whereas the impact of in vivo BET inhibition on tumor immunity (Hogg et al., 2017; Mao et al., 2019; Zhu et al., 2016), especially antitumor CD8 T cells, remains unclear. Given that *Brd4* knockdown and JQ1 treatment constrained CD8 T cell differentiation during infection and within tumors, we tested if we could leverage these findings to modulate the efficacy of promising immunotherapy approaches, such as adoptive cell therapy and immune checkpoint blockade. We first tested how JQ1 treatment impacted the efficacy of adoptive cell therapy in a widely used and characteristically immunosuppressive B16 melanoma tumor model (Fig. 5 D; Chen et al., 2015; Juneja et al., 2017; Kleffel et al., 2015). Upon adoptive transfer of tumor-specific T cells into immunocompetent mice bearing established melanoma tumors, we found that tumor growth was delayed in vehicle-treated mice that received antitumor P14 cells compared with mice that did not receive P14 T cells, as expected (Fig. 5 D and Fig. S3 B); however, JQ1 treatment resulted in diminished efficacy of transferred tumor-specific P14 cells, ultimately yielding similar tumor growth rates to that of recipient mice without P14 cells (Fig. 5 D and Fig. S3 B). Further evaluation of the phenotype of adoptively transferred cells in JQ1-treated mice or P14 cells deficient for BRD4 revealed failed production of the essential cytolytic molecule GzB (Fig. 5 E), a direct target of BRD4 (Fig. 4 H) characteristically expressed by terminally exhausted cells (Miller et al., 2019; Milner et al., 2020b; Siddiqui et al., 2019). Furthermore, daily JQ1 treatment resulted in nearly 10-fold fewer P14 cells in the tumor microenvironment (Fig. S3 C). These findings highlight a scenario wherein BET inhibition of terminal CD8 T cell differentiation may be problematic in an adoptive cell therapy setting or perhaps in patients with a robust antitumor CD8 T cell response. These results can be partially explained by the finding that terminally exhausted cells produce more GzB and exhibit superior antitumor cytotoxicity compared with progenitor-exhausted cells (Miller et al., 2019), despite their short-lived and terminal phenotype. It is important to note that, although the phenotype of tumor-specific T cells in JQ1-treated mice is similar to the phenotype detected with cell-intrinsic *Brd4* RNAi studies, BET inhibition may also indirectly impact CD8 T cell responses through modulating the activity of BET proteins in other cell types.

We speculated that the fairly aggressive regimen of daily 50 mg/kg JQ1 treatment in Fig. 5 D may excessively limit T cell differentiation and effector capacity, and we next evaluated a lower dose of 10 mg/kg JQ1. In vivo treatment with 10 mg/kg JQ1 resulted in a reduced frequency of Tim3^{hi} tumor-specific cells (Fig. 5 F) and a greater frequency of TCF1^{hi} cells (Fig. S3 D) compared with vehicle-treated mice, but not to the same extent as that for 50 mg/kg JQ1. Given that terminally differentiated CD8 T cells exhibit a fixed epigenetic state that limits longevity and responsiveness to immunotherapies, such as immune checkpoint blockade (Fig. S1 A; Pauken et al., 2016; Philip et al., 2017; Siddiqui et al., 2019), we next tested if a 10-mg/kg JQ1 treatment course may allow for enhanced efficacy of α-PD-1 therapy through the blunting of terminal differentiation of P14 cells in tumors. Here, we used an MC38 colon carcinoma model with known sensitivity to α-PD-1 therapy (Juneja et al., 2017). Indeed, we found a 10-mg/kg JQ1 treatment regimen enhanced the efficacy of α-PD-1, wherein only ∼17% of vehicle-treated mice responded to α-PD-1 therapy compared with nearly 50%

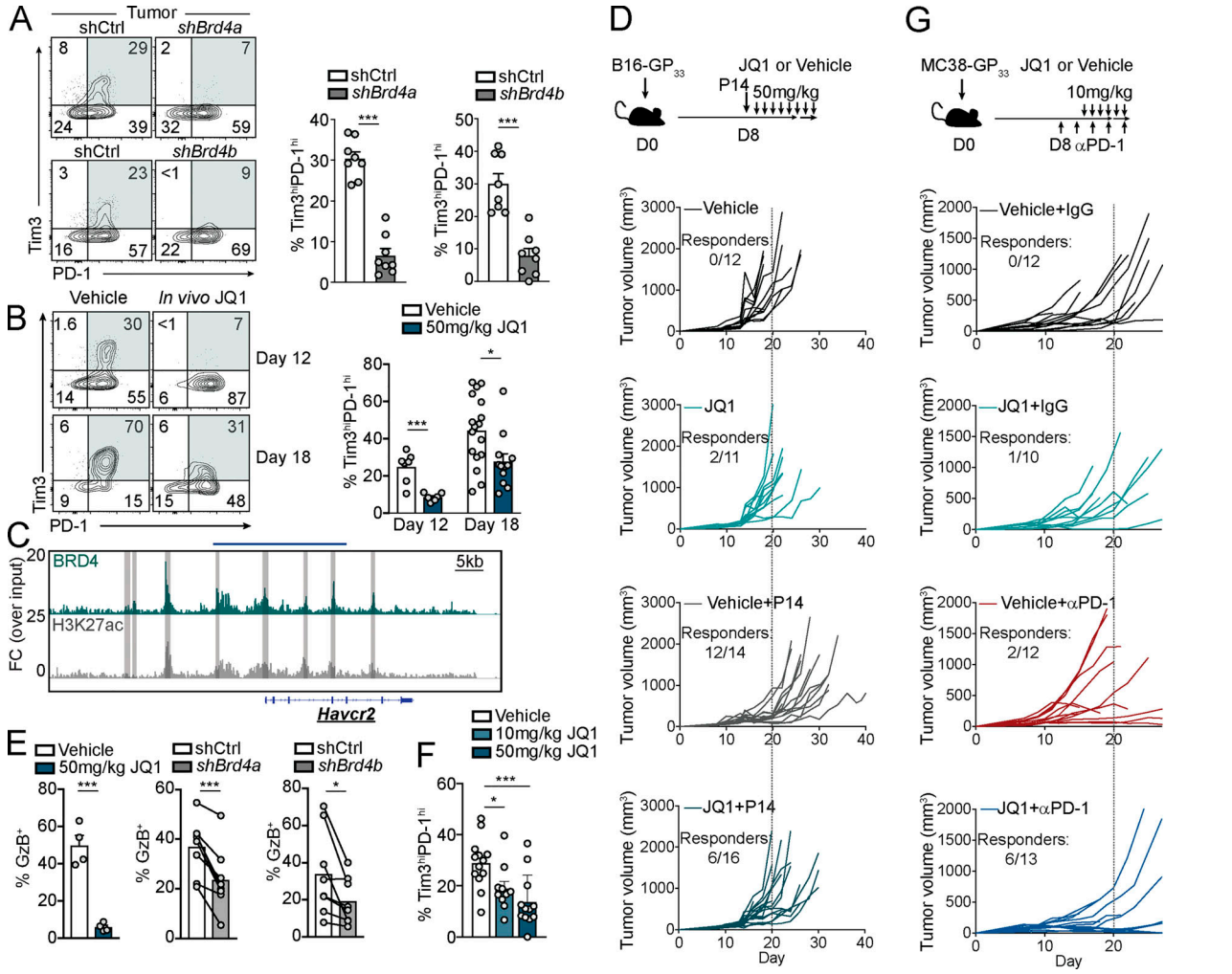

Figure 5. **BRD4 regulates CD8 T cell differentiation during cancer. (A)** Experimental schematic (left) wherein congenically distinct P14 cells were transduced with *Brd4* shRNA–encoding or control shRNA–encoding retroviruses. Transduced cells were transferred into mice bearing established B16-GP_{33-41} tumors as in Fig. S3 A. Representative flow cytometry plots (left) and quantification (right) of the frequency of *shBrd4* or shCtrl cells on days 11 or 12 after transplant. **(B)** P14 cells were transferred into recipient mice bearing established B16-GP_{33-41} tumors, and recipient mice were treated daily with 50 mg/kg JQ1 or vehicle daily. Frequency of PD-$1^{hi}Tim3^{hi}$ P14 cells on days 12 and 18 after transplant. **(C)** Representative TE H3K27ac and BRD4 peaks near *Havcr2* (encoding Tim3). A super-enhancer region is demarcated with a blue line above the tracks. Reproducible BRD4 peaks are highlighted (gray) using the ENCODE ChIP-seq pipeline. **(D)** P14 cells were adoptively transferred to B16-GP_{33-41} tumor-bearing mice subsequently treated with JQ1 (50 mg/kg) or vehicle daily for the first week after adoptive transfer and then every other day thereafter. Tumor volume was assessed and responders were defined as mice with a nonulcerated tumor <500 mm^3 on day 20 after transplant. **(E)** Frequency of GzB-expressing P14 cells from experimental setup in A or B. **(F)** P14 cells were adoptively transferred to B16-GP_{33-41} tumor-bearing mice that were subsequently treated with 50 mg/kg JQ1, 10 mg/ml JQ1, or vehicle daily and the frequency of PD-$1^{hi}Tim3^{hi}$ cells was evaluated. **(G)** MC38-GP_{33-41} tumor-bearing mice were treated with 0.2 mg α-PD-1 every 2 d beginning on day 8 after transplant and 10 mg/kg JQ1 daily beginning on day 11 after transplant. Tumor volume was assessed and responders were defined as mice with a nonulcerated tumor <200 mm^3 on day 27 after transplant. Graphs show mean ± SEM of n = 6–17 pooled from two to four independent studies (A, B, and D–G) or n = 4 from one representative of two independent studies (E, left). *, P < 0.05; ***, P < 0.005. Symbols represent an individual mouse (A, B, E, and F).

of mice responding to α-PD-1 in combination with 10-mg/kg JQ1 treatment (Fig. 5 G). These data highlight that resolving the roles BET proteins and their degree of activity in antitumor CD8 T cells may yield insight into enhancing BET therapy efficacy and synergy, which is particularly relevant given that early findings from clinical studies of BET inhibitors as a cancer monotherapy leave room for improvement (Khandekar and Tiriveedhi, 2020).

This investigation provides insight into how complex chromatin dynamics accompanying CD8 T cell differentiation are interpreted and conveyed during infection. We established that BRD4 binds to gene bodies, traditional enhancers, and super-enhancers to regulate the expression of genes critical to effector differentiation and identity, including pro-effector transcription factors (*Id2*, *Bhlhe40*, *Zeb2*, and *Runx1*), effector molecules (*Gzma*, *Gzmb*, and *Fasl*), and canonical TE-surface molecules or mediators of cell trafficking (*Klrg1*, *Cx3cr1*, *Itgam*, *Ccr5*, and *Ly6c2*). *Brd4* expression is relatively uniform among diverse CD8 T cell populations, highlighting the utility of our RNAi screening strategy and indicating that the fate-specifying activity of BRD4 is likely dictated by the cis regulatory landscape as CD8 T cells gain nearly twofold more de novo enhancer

regions during their transition from a naive cell to a TE cell state compared with an MP state (Yu et al., 2017). BRD4 activity may also be regulated by post-translational modifications (Shu et al., 2016; Wu et al., 2013) and/or interactions with other regulatory molecules, such as mediators of transcription elongation (Chen et al., 2014; Jang et al., 2005; Yang et al., 2005). BRD4 is widely classified as a chromatin reader, but has diverse functions ranging from kinase activity (Devaiah et al., 2012) to binding nonhistone acetylated molecules, such as p65 (Huang et al., 2009). While it is possible that BRD4 controls T cell fate during infection and cancer through a range of actions, assessment of genome-wide binding patterns indicates that a primary function of BRD4 in CD8 T cells is regulating expression of key genes through supporting transcription of gene bodies directly and promoting activity of super-enhancers. Taken together, we identify BRD4 as a critical regulator of CD8 T cell differentiation and function during infection and cancer.

Materials and methods

Mice

All mice were bred and housed in specific pathogen–free conditions in accordance with the Institutional Animal Care and Use Guidelines of the University of California San Diego or the National Institute of Child Health and Human Development. P14 mice (with transgenic expression of H-2D^b–restricted TCR specific for LCMV glycoprotein GP$_{33-41}$), *Brd4*$^{fl/fl}$ *Ert2*$^{Cre/+}$ (Dey et al., 2019), and CD45.1 and CD45.2 congenic mice were bred in-house. Male and female mice were used with sex-matched T cell donors and recipients or female cells were transferred into male recipients.

T cell transfers, bone marrow chimeras, infections, and treatments

For BET inhibition studies, naive P14 cells (5×10^4) were transferred into congenically distinct recipient mice subsequently infected with 2×10^5 PFU of LCMV by i.p. injection. The following BET inhibitors were used in this study: JQ1 (prepared by the laboratory of Jun Qi), OTX-015 (MedChemExpress), and MS402 (prepared by the laboratory of Ming-Ming Zhou). A concentrated stock of JQ1 in DMSO was prepared at 50 mg/ml and diluted 1:10 in 10% cyclodextrin, and mice received 50 mg/kg or 10 mg/kg via i.p. injection as indicated. A concentrated stock of OTX-015 in DMSO was prepared at 50 mg/ml and diluted in sunflower oil, and 50 mg/kg was administered via oral gavage. A concentrated stock of MS402 in DMSO was prepared at 20 mg/ml and diluted in 10% cyclodextrin, and 40 mg/kg was administered i.p. Administered vehicle control for all inhibitors was DMSO in 10% cyclodextrin (i.p injections) or sunflower oil (oral gavage treatments).

Mixed bone marrow chimera mice were established by transferring a 1:1 mix of *Brd4*$^{fl/fl}$*Ert2*$^{Cre/+}$ bone marrow cells with congenically distinct WT *Brd4*$^{+/+}$ bone marrow cells into irradiated congenically distinct recipient mice. After reconstitution (~12 wk after transfer), chimeric mice were then infected with LCMV. For ER-Cre–mediated deletion of floxed alleles, 2 mg tamoxifen (Cayman Chemical Company) was administered daily by i.p. injection for 3–5 consecutive days at various time points after infection.

In vivo RNAi screen

The pooled in vivo shRNAmir screen was performed similarly as previously described (Milner et al., 2017). Briefly, P14 cells were activated in 96-well plates, individually transduced with 215 distinct shRNAmir encoding retroviruses, pooled, and 5×10^5 total P14 cells were transferred into 15–18 recipient mice subsequently infected with LCMV. Twelve days after infection, CD62L^{hi} and CD62L^{lo} splenic P14 cells were sorted and genomic DNA was harvested. Proviral passenger strand shRNAmir sequences were PCR amplified, and a minimum of 2.5 million reads per sample were generated and retained after filtering low-quality reads. shRNAmir representation in CD62L^{lo} cells relative to CD62L^{hi} cells was calculated by normalizing the total number of reads in each of the samples, and then the number of reads for each shRNAmir was scaled proportionally. Subsequently, the normalized number of reads in the CD62L^{lo} cells for a given shRNAmir was divided by the normalized number of reads for the same shRNAmir in the CD62L^{hi} cell sample and then $\log_2$ transformed. Mean and SD of the ratios of 25 negative control shRNAmir constructs (targeting *Cd19*, *Cd4*, *Cd14*, *Ms4a1*, *Cd22*, *Hes1*, *Klf12*, *Mafb*, *Plagl1*, *Pou2af1*, and *Smarca1*) were used to calculate the Z-score for each shRNAmir. The in vivo screen was repeated three times and the Z-score of each construct from each individual screen was averaged. All constructs were screened two to three times (except for 13 constructs, which are marked by an asterisk in Table S1) as certain constructs were added after the first screen or were not detectable in one of the replicate experiments.

In vivo *Brd2* and *Brd4* RNAi during LCMV infection

For in vivo *Brd2* and *Brd4* RNAi experiments, two distinct shRNAmir clones for each gene were used in our previously described pLMPd-Amt vector (Chen et al., 2014; Wang et al., 2018), and retroviral supernatant was produced as described previously (Milner et al., 2017). For transfections, Plat-E cells were seeded in 10-cm dishes at a density of 2.5×10^5 cells/plate 1 d before transfection in serum-free media. Transfections were performed with 100 µg plasmid DNA from each pLMPd-Amt clone and 50 µg pCL-Eco with TransIT-LT1 (Mirus). Retroviral supernatant was harvested 48 h and 72 h after transfection. For transductions, negatively enriched naive CD8 T cells from spleen and lymph nodes were activated in 6-well plates coated with 100 µg/ml goat anti-hamster IgG (H+L; Thermo Fisher Scientific), 1 µg/ml anti-CD3 (145-2C11; eBioscience), and 1 µg/ml anti-CD28 (37.51; eBioscience). T cell culture media was removed 18 h after activation and replaced with retroviral supernatant supplemented with 50 µM β-mercaptoethanol (Gibco) and 8 µg/ml polybrene (Millipore) followed by a 1 h spinfection centrifugation at 2,000 rpm and 37°C. One day after transduction, congenically distinct ametrine$^+$ T cells were mixed 1:1 and 5×10^5 total cells were transferred into recipient mice subsequently infected with LCMV.

Tumor models

Tumors were established by transplanting 5×10^5 B16-GP$_{33-41}$ cells or $2.5–5 \times 10^5$ MC38-GP$_{33-41}$ cells subcutaneously. Cell lines was treated for mycoplasma contamination and authenticated in

in vitro killing assays. P14 cells were in vitro expanded in IL-2 (100 mg/ml) for 2–4 d, after which 1–2 × 10^6 cells (or 4 × 10^6 cells; Fig. 5 D) were transferred into congenically distinct tumor-bearing mice 7–8 d after transplant. Mice were treated with JQ1 or vehicle as described above. *Brd4* RNAi experiments in tumors were performed as described above, except transduced cells were cultured for 2–3 d after transduction before mixed transfer. For immune checkpoint blockade studies, 0.2 mg of α-PD-1 or isotype control were administered i.p. every other day beginning on day 7/8 after transplant. Tumors were monitored every 2–3 d, and mice with ulcerated tumors or tumors exceeding 1,500 mm^3 were euthanized, in accordance with the Institutional Animal Care and Use Guidelines of the University of California San Diego. TILs were isolated as previously described (Milner et al., 2017).

Antibodies, intracellular staining, flow cytometry, and cell sorting

Single-cell suspensions were prepared from spleen or lymph node by mechanical disruption, and intestinal tissue and tumor were processed as described previously (Milner et al., 2017). RBCs were lysed with ACK buffer (140 mM NH_4Cl and 17 mM Tris-base, pH 7.4). The following antibodies were used for surface staining (all from eBioscience unless otherwise specified): CD8 (53–6.7), CD27 (LG-7F9), CD43 (eBioR2.60), CD44 (IM7), CD45.1 (A20-1.7), CD45.2 (104), CD69 (H1.2F3; BioLegend), CD103 (2E7), Tim3 (RMT3-23), CD127 (A7R34), CD62L (MEL-14), KLRG1 (2F1), PD-1 (J43), and CX3CR1 (SA011F11; BioLegend); or intracellular staining: GzB (GB12; Invitrogen), Eomes (Dan11-mag), TCF1 (C63D9; Cell Signaling Technology), T-bet (4B10), and Ki-67 (SolA15). The H-$2D^b$-GP_{33-41} tetramer was obtained from the National Institutes of Health Tetramer Core. Intracellular staining was performed using the Foxp3 Transcription Factor Staining Buffer Set (eBioscience). CellTrace Violet (Ebioscience) and BrdU (BD PharMingen) were used per manufacturer instructions where 2 mg BrdU was administered i.p. 2 h before tissue harvesting. For flow cytometry analysis, all data were acquired on a BD LSRFortessa X-20 or a BD LSRFortessa. Cell sorting was performed on BD FACSAria or BD FACSAria Fusion instruments.

Quantitative PCR and RNA sequencing

For validation of *Brd2* and *Brd4* knockdown with shRNAmir constructs, enriched $CD8^+$ T cells were activated, transduced, and expanded for 4–6 d in 100 mg/ml IL-2. Ametrine$^+$ cells (*Brd2 shRNAmir*, *Brd4* shRNAmir, or control *Cd19* shRNAmir) were sorted directly into TRIzol (Life Technologies) and RNA was extracted per manufacturer specifications. cDNA was then synthesized using Superscript II (Life Technologies) and quantitative PCR was performed using the Stratagene Brilliant II Syber Green master mix (Agilent Technologies). *Brd2 and Brd4* expression levels were normalized to the housekeeping genes *Hprt1 or Gapdh*. The following primers were used for quantitative PCR: *Brd2* forward: 5′-GCTGAGCGGCGGCGGTTCCC-3′, and *Brd2* reverse: 5′-GTAAAG CTGGTACAGAAGCC-3′; *Brd4* forward: 5′-TTCAGCACCTCACTTCGA CC-3′, and *Brd4* reverse: 5′-CTGGTG TTTTTGGCTCCTGC-3′; *Hprt* forward: 5′-GGCCAGACTTTGTTG GATTT-3′, and *Hprt* reverse: 5′-CAACTTGCGCTCATCTTAGG-3′; and *Gapdh* forward: 5′-CCAGTATGACTC CACTCACG-3′, and *Gapdh* reverse: 5′-GACTCCACGACATACTCAGC-3′.

For RNA sequencing studies, 10^3 P14 cells were sorted on day 5 of infection or tetramer$^+$ cells were sorted on day 8 of infection. RNA sequencing was performed in duplicate or triplicate wherein day 5 JQ1/vehicle or *shBrd4*/shCtrl P14 replicates or day 8 tetramer$^+$ replicates were sorted from cells pooled from two mice (i.e., each replicate was composed of cells from two separate mice). For all samples, polyA$^+$ RNA was isolated and RNA sequencing library preparation and RNA sequencing analysis were performed as described (https://www.immgen.org/Protocols/11Cells.pdf). Heatmaps were generated using Morpheus (https://software.broadinstitute.org/morpheus). Gene set enrichment analysis was performed with gene set enrichment analysis v4.0.3: Number of permutations = 1,000, permutation type = gene_set, enrichment statistic = weighted, metric for ranking genes = Signal2Noise. MP, TE, and EEC signature gene sets were generated by identifying genes differentially expressed between each subset in WT tetramer$^+$ cells on day 8 of infection (1.5-fold change, expression threshold ≥ 10).

BRD4 ChIP-seq

For ChIP-seq studies, 10^5 naive P14 cells were transferred to recipient mice subsequently infected i.p. with 2 × 10^5 PFU of the Armstrong strain of LCMV 1 d after cell transfer. Negatively enriched splenocytes were sorted for TE cells (KLRG1$^+$CD127$^-$) on day 8 after infection. Duplicate samples were prepared for subsequent ChIP-seq analyses, wherein each replicate consisted of 1.5 × 10^7 TE cells pooled from five mice. Cells were then fixed by adding 1/10 volume of freshly prepared 37% formaldehyde (#F-8775; Sigma-Aldrich) for 15 min. Fixation was then stopped by adding 1/20 volume of 2.5 M Glycine for 5 min. Cells were washed with chilled 0.5% Igepal/PBS and 1 mM PMSF, and then cell pellets were flash frozen and shipped to Active Motif for anti-BRD4 (Bethyl A301-985A100) ChIP-seq. For BRD4 ChIP reactions, 25 µg chromatin and 6 µl antibody were used. Fastq files for H3K27ac ChIP-seq in TE OT-I cells were downloaded from the Gene Expression Omnibus (accession no. GSE89036). The Fastq files for BRD4 from Active Motif and for H3K27ac ChIP-seq were analyzed through the Chip-seq pipeline from Encode (https://www.encodeproject.org/pipelines/), and the reproducible peak sets along with the bigwig tracks of fold change over background were used. The ROSE algorithm (Lovén et al., 2013; Whyte et al., 2013) was used to identify super-enhancers from the H3K27ac peak set. Homer was used to annotate the peak sets and compare BRD4 binding and super-enhancer locations (http://homer.ucsd.edu/homer/).

Statistics

Statistical analysis was performed using GraphPad Prism software. Two-tailed paired or unpaired *t* test was used for comparisons between two groups. P values of <0.05 were considered significant. Log-rank (Mantel-Cox) test was used to compare survival curves.

Online supplemental material

Fig. S1 provides supporting information on the efficacy of *Brd4* RNAi and inducible floxed models, as well as further phenotyping of *Brd4*-deficient CD8 T cells. Fig. S2 illustrates expression patterns of BET proteins in CD8 T cell populations during LCMV infection and provides information on the phenotype of *Brd2*-deficient CD8 T cells. Fig. S3 lists details on the phenotype of *Brd4*-deficient T cells in mouse melanoma tumors. Table S1 shows summary Z-scores from the in vivo RNAi screening approach.

Data availability

All RNA sequencing and ChIP-seq datasets have been deposited in the Gene Expression Omnibus under accession no. GSE173515 (and subseries GSE173510, GSE173511, GSE173512, and GSE173513).

Acknowledgments

Fig. 1 A schematic was generated with Biorender.com.

This work was funded by National Institutes of Health grants AI132122 (A.W. Goldrath), U19AI109976 (A.W. Goldrath, M.E. Pipkin, and S. Crotty), K99/R00 CA234430-01 (J.J. Milner), and R01AI130152 (T. Egawa), the Leukemia and Lymphoma Society Scholar Award (T. Egawa) and a Cancer Research Institute Postdoctoral Fellowship (M. Reina-Campos).

Author contributions: Conceptualization: J.J. Milner and A.W. Goldrath; methodology and reagents: J.J. Milner, C. Toma, S. Quon, A. Dey, M. Reina-Campos, A.J. Getzler, H. Diao, B. Yu, A. Delpoux, D. Li, J. Qi, A. Vincek, S.M. Hedrick, T. Egawa, M.-M. Zhou, S. Crotty, K. Ozato, M.E. Pipkin, and A.W. Goldrath; investigation: J.J. Milner, C. Toma, S. Quon, K. Omilusik, N.E. Scharping, M. Reina-Campos, H. Nguyen, T.M. Yoshida, S. Crotty, M.E. Pipkin, and A.W. Goldrath; formal analysis: J.J. Milner, S. Quon, N.E. Scharping, M. Reina-Campos, A.J. Getzler, H. Diao, M.E. Pipkin, and A.W. Goldrath; writing: J.J. Milner, M.E. Pipkin, and A.W. Goldrath; funding acquisition: J.J. Milner, S. Crotty, M.E. Pipkin, and A.W. Goldrath.

A.W. Goldrath reported “other” from Pandion Therapeutics and “other” from ArsenalBio outside the submitted work, and is on the SAB of Pandion Therapeutics and ArsenalBio. J. Qi reported “other” from Epiphanes outside the submitted work. No other disclosures were reported.

Submitted: 24 November 2020
Revised: 10 March 2021
Accepted: 3 May 2021

References

Bai, A., H. Hu, M. Yeung, and J. Chen. 2007. Kruppel-like factor 2 controls T cell trafficking by activating L-selectin (CD62L) and sphingosine-1-phosphate receptor 1 transcription. *J. Immunol.* 178:7632–7639. https://doi.org/10.4049/jimmunol.178.12.7632

Bandukwala, H.S., J. Gagnon, S. Togher, J.A. Greenbaum, E.D. Lamperti, N.J. Parr, A.M. Molesworth, N. Smithers, K. Lee, J. Witherington, et al. 2012. Selective inhibition of CD4+ T-cell cytokine production and autoimmunity by BET protein and c-Myc inhibitors. *Proc. Natl. Acad. Sci. USA.* 109:14532–14537. https://doi.org/10.1073/pnas.1212264109

Boi, M., E. Gaudio, P. Bonetti, I. Kwee, E. Bernasconi, C. Tarantelli, A. Rinaldi, M. Testoni, L. Cascione, M. Ponzoni, et al. 2015. The BET bromodomain inhibitor OTX015 affects pathogenetic pathways in preclinical B-cell tumor models and synergizes with targeted drugs. *Clin. Cancer Res.* 21:1628–1638. https://doi.org/10.1158/1078-0432.CCR-14-1561

Böttcher, J.P., M. Beyer, F. Meissner, Z. Abdullah, J. Sander, B. Höchst, S. Eickhoff, J.C. Rieckmann, C. Russo, T. Bauer, et al. 2015. Functional classification of memory CD8(+) T cells by CX3CR1 expression. *Nat. Commun.* 6:8306. https://doi.org/10.1038/ncomms9306

Cannarile, M.A., N.A. Lind, R. Rivera, A.D. Sheridan, K.A. Camfield, B.B. Wu, K.P. Cheung, Z. Ding, and A.W. Goldrath. 2006. Transcriptional regulator Id2 mediates CD8+ T cell immunity. *Nat. Immunol.* 7:1317–1325. https://doi.org/10.1038/ni1403

Chang, J.T., E.J. Wherry, and A.W. Goldrath. 2014. Molecular regulation of effector and memory T cell differentiation. *Nat. Immunol.* 15:1104–1115. https://doi.org/10.1038/ni.3031

Chee, J., C. Wilson, A. Buzzai, B. Wylie, C.A. Forbes, M. Booth, N. Principe, B. Foley, M.N. Cruickshank, and J. Waithman. 2020. Impaired T cell proliferation by *ex vivo* BET-inhibition impedes adoptive immunotherapy in a murine melanoma model. *Epigenetics.* 15:134–144. https://doi.org/10.1080/15592294.2019.1656156

Chen, R., S. Bélanger, M.A. Frederick, B. Li, R.J. Johnston, N. Xiao, Y.-C. Liu, S. Sharma, B. Peters, A. Rao, et al. 2014. In vivo RNA interference screens identify regulators of antiviral CD4(+) and CD8(+) T cell differentiation. *Immunity.* 41:325–338. https://doi.org/10.1016/j.immuni.2014.08.002

Chen, S., L.F. Lee, T.S. Fisher, B. Jessen, M. Elliott, W. Evering, K. Logronio, G.H. Tu, K. Tsaparikos, X. Li, et al. 2015. Combination of 4-1BB agonist and PD-1 antagonist promotes antitumor effector/memory CD8 T cells in a poorly immunogenic tumor model. *Cancer Immunol. Res.* 3:149–160. https://doi.org/10.1158/2326-6066.CIR-14-0118

Cheung, K., G. Lu, R. Sharma, A. Vincek, R. Zhang, A.N. Plotnikov, F. Zhang, Q. Zhang, Y. Ju, Y. Hu, et al. 2017a. BET N-terminal bromodomain inhibition selectively blocks Th17 cell differentiation and ameliorates colitis in mice. *Proc. Natl. Acad. Sci. USA.* 114:2952–2957. https://doi.org/10.1073/pnas.1615601114

Cheung, K.L., F. Zhang, A. Jaganathan, R. Sharma, Q. Zhang, T. Konuma, T. Shen, J.-Y. Lee, C. Ren, C.-H. Chen, et al. 2017b. Distinct roles of Brd2 and Brd4 in potentiating the transcriptional program for Th17 cell differentiation. *Mol. Cell.* 65:1068–1080.e5. https://doi.org/10.1016/j.molcel.2016.12.022

Cochran, A.G., A.R. Conery, and R.J. Sims III. 2019. Bromodomains: a new target class for drug development. *Nat. Rev. Drug Discov.* 18:609–628. https://doi.org/10.1038/s41573-019-0030-7

Cui, W., Y. Liu, J.S. Weinstein, J. Craft, and S.M. Kaech. 2011. An interleukin-21-interleukin-10-STAT3 pathway is critical for functional maturation of memory CD8+ T cells. *Immunity.* 35:792–805. https://doi.org/10.1016/j.immuni.2011.09.017

Delmore, J.E., G.C. Issa, M.E. Lemieux, P.B. Rahl, J. Shi, H.M. Jacobs, E. Kastritis, T. Gilpatrick, R.M. Paranal, J. Qi, et al. 2011. BET bromodomain inhibition as a therapeutic strategy to target c-Myc. *Cell.* 146:904–917. https://doi.org/10.1016/j.cell.2011.08.017

Devaiah, B.N., B.A. Lewis, N. Cherman, M.C. Hewitt, B.K. Albrecht, P.G. Robey, K. Ozato, R.J. Sims III, and D.S. Singer. 2012. BRD4 is an atypical kinase that phosphorylates serine2 of the RNA polymerase II carboxy-terminal domain. *Proc. Natl. Acad. Sci. USA.* 109:6927–6932. https://doi.org/10.1073/pnas.1120422109

Dey, A., W. Yang, A. Gegonne, A. Nishiyama, R. Pan, R. Yagi, A. Grinberg, F.D. Finkelman, K. Pfeifer, J. Zhu, et al. 2019. BRD4 directs hematopoietic stem cell development and modulates macrophage inflammatory responses. *EMBO J.* 38:e100293. https://doi.org/10.15252/embj.2018100293

Diao, H., and M. Pipkin. 2019. Stability and flexibility in chromatin structure and transcription underlies memory CD8 T-cell differentiation. *F1000 Res.* 8:1278. https://doi.org/10.12688/f1000research.18211.1

Dominguez, C.X., R.A. Amezquita, T. Guan, H.D. Marshall, N.S. Joshi, S.H. Kleinstein, and S.M. Kaech. 2015. The transcription factors ZEB2 and T-bet cooperate to program cytotoxic T cell terminal differentiation in response to LCMV viral infection. *J. Exp. Med.* 212:2041–2056. https://doi.org/10.1084/jem.20150186

Donati, B., E. Lorenzini, and A. Ciarrocchi. 2018. BRD4 and Cancer: going beyond transcriptional regulation. *Mol. Cancer.* 17:164. https://doi.org/10.1186/s12943-018-0915-9

Filippakopoulos, P., J. Qi, S. Picaud, Y. Shen, W.B. Smith, O. Fedorov, E.M. Morse, T. Keates, T.T. Hickman, I. Felletar, et al. 2010. Selective inhibition of BET bromodomains. *Nature.* 468:1067–1073. https://doi.org/10.1038/nature09504

Georgiev, P., Y. Wang, E.S. Muise, M.L. Bandi, W. Blumenschein, M. Sathe, E.M. Pinheiro, and S.D. Shumway. 2019. BET Bromodomain Inhibition Suppresses Human T Cell Function. *Immunohorizons.* 3:294–305. https://doi.org/10.4049/immunohorizons.1900037

Gerlach, C., E.A. Moseman, S.M. Loughhead, D. Alvarez, A.J. Zwijnenburg, L. Waanders, R. Garg, J.C. de la Torre, and U.H. von Andrian. 2016. The Chemokine Receptor CX3CR1 Defines Three Antigen-Experienced CD8 T Cell Subsets with Distinct Roles in Immune Surveillance and Homeostasis. *Immunity.* 45:1270–1284. https://doi.org/10.1016/j.immuni.2016.10.018

Hart, G.T., K.A. Hogquist, and S.C. Jameson. 2012. Krüppel-like factors in lymphocyte biology. *J. Immunol.* 188:521–526. https://doi.org/10.4049/jimmunol.1101530

He, B., S. Xing, C. Chen, P. Gao, L. Teng, Q. Shan, J.A. Gullicksrud, M.D. Martin, S. Yu, J.T. Harty, et al. 2016. CD8+ T cells utilize highly dynamic enhancer repertoires and regulatory circuitry in response to infections. *Immunity.* 45:1341–1354. https://doi.org/10.1016/j.immuni.2016.11.009

Hess Michelini, R., A.L. Doedens, A.W. Goldrath, and S.M. Hedrick. 2013. Differentiation of CD8 memory T cells depends on Foxo1. *J. Exp. Med.* 210:1189–1200. https://doi.org/10.1084/jem.20130392

Hogg, S.J., S.J. Vervoort, S. Deswal, C.J. Ott, J. Li, L.A. Cluse, P.A. Beavis, P.K. Darcy, B.P. Martin, A. Spencer, et al. 2017. BET-bromodomain inhibitors engage the host immune system and regulate expression of the immune checkpoint ligand PD-L1. *Cell Rep.* 18:2162–2174. https://doi.org/10.1016/j.celrep.2017.02.011

Huang, B., X.-D. Yang, M.-M. Zhou, K. Ozato, and L.-F. Chen. 2009. Brd4 coactivates transcriptional activation of NF-kappaB via specific binding to acetylated RelA. *Mol. Cell. Biol.* 29:1375–1387. https://doi.org/10.1128/MCB.01365-08

Ichii, H., A. Sakamoto, M. Hatano, S. Okada, H. Toyama, S. Taki, M. Arima, Y. Kuroda, and T. Tokuhisa. 2002. Role for Bcl-6 in the generation and maintenance of memory CD8+ T cells. *Nat. Immunol.* 3:558–563. https://doi.org/10.1038/ni802

Im, S.J., M. Hashimoto, M.Y. Gerner, J. Lee, H.T. Kissick, M.C. Burger, Q. Shan, J.S. Hale, J. Lee, T.H. Nasti, et al. 2016. Defining CD8+ T cells that provide the proliferative burst after PD-1 therapy. *Nature.* 537:417–421. https://doi.org/10.1038/nature19330

Jameson, S.C., and D. Masopust. 2018. Understanding Subset Diversity in T Cell Memory. *Immunity.* 48:214–226. https://doi.org/10.1016/j.immuni.2018.02.010

Jang, M.K., K. Mochizuki, M. Zhou, H.-S. Jeong, J.N. Brady, and K. Ozato. 2005. The bromodomain protein Brd4 is a positive regulatory component of P-TEFb and stimulates RNA polymerase II-dependent transcription. *Mol. Cell.* 19:523–534. https://doi.org/10.1016/j.molcel.2005.06.027

Ji, Y., Z. Pos, M. Rao, C.A. Klebanoff, Z. Yu, M. Sukumar, R.N. Reger, D.C. Palmer, Z.A. Borman, P. Muranski, et al. 2011. Repression of the DNA-binding inhibitor Id3 by Blimp-1 limits the formation of memory CD8+ T cells. *Nat. Immunol.* 12:1230–1237. https://doi.org/10.1038/ni.2153

Joshi, N.S., W. Cui, A. Chandele, H.K. Lee, D.R. Urso, J. Hagman, L. Gapin, and S.M. Kaech. 2007. Inflammation directs memory precursor and short-lived effector CD8(+) T cell fates via the graded expression of T-bet transcription factor. *Immunity.* 27:281–295. https://doi.org/10.1016/j.immuni.2007.07.010

Juneja, V.R., K.A. McGuire, R.T. Manguso, M.W. LaFleur, N. Collins, W.N. Haining, G.J. Freeman, and A.H. Sharpe. 2017. PD-L1 on tumor cells is sufficient for immune evasion in immunogenic tumors and inhibits CD8 T cell cytotoxicity. *J. Exp. Med.* 214:895–904. https://doi.org/10.1084/jem.20160801

Kaech, S.M., J.T. Tan, E.J. Wherry, B.T. Konieczny, C.D. Surh, and R. Ahmed. 2003. Selective expression of the interleukin 7 receptor identifies effector CD8 T cells that give rise to long-lived memory cells. *Nat. Immunol.* 4:1191–1198. https://doi.org/10.1038/ni1009

Kagoya, Y., M. Nakatsugawa, Y. Yamashita, T. Ochi, T. Guo, M. Anczurowski, K. Saso, M.O. Butler, C.H. Arrowsmith, and N. Hirano. 2016. BET bromodomain inhibition enhances T cell persistence and function in adoptive immunotherapy models. *J. Clin. Invest.* 126:3479–3494. https://doi.org/10.1172/JCI86437

Kallies, A., A. Xin, G.T. Belz, and S.L. Nutt. 2009. Blimp-1 transcription factor is required for the differentiation of effector CD8(+) T cells and memory responses. *Immunity.* 31:283–295. https://doi.org/10.1016/j.immuni.2009.06.021

Kallies, A., D. Zehn, and D.T. Utzschneider. 2020. Precursor exhausted T cells: key to successful immunotherapy? *Nat. Rev. Immunol.* 20:128–136. https://doi.org/10.1038/s41577-019-0223-7

Khandekar, D., and V. Tiriveedhi. 2020. Role of BET inhibitors in triple negative breast cancers. *Cancers (Basel).* 12:784. https://doi.org/10.3390/cancers12040784

Kim, M.V., W. Ouyang, W. Liao, M.Q. Zhang, and M.O. Li. 2013. The transcription factor Foxo1 controls central-memory CD8+ T cell responses to infection. *Immunity.* 39:286–297. https://doi.org/10.1016/j.immuni.2013.07.013

Kleffel, S., C. Posch, S.R. Barthel, H. Mueller, C. Schlapbach, E. Guenova, C.P. Elco, N. Lee, V.R. Juneja, Q. Zhan, et al. 2015. Melanoma Cell-Intrinsic PD-1 Receptor Functions Promote Tumor Growth. *Cell.* 162:1242–1256. https://doi.org/10.1016/j.cell.2015.08.052

Knell, J., J.A. Best, N.A. Lind, E. Yang, L.M. D'Cruz, and A.W. Goldrath. 2013. Id2 influences differentiation of killer cell lectin-like receptor G1(hi) short-lived CD8+ effector T cells. *J. Immunol.* 190:1501–1509. https://doi.org/10.4049/jimmunol.1200750

Kurd, N., Z. He, J. Milner, K. Omilusik, T. Louis, M. Tsai, C. Widjaja, J. Kanbar, J. Olvera, and T. Tysl. 2020. Molecular determinants and heterogeneity of tissue-resident memory CD8+ T lymphocytes revealed by single-cell RNA sequencing. *bioRxiv.* https://doi.org/10.1101/2020.03.02.973578

Lee, J.-E., Y.-K. Park, S. Park, Y. Jang, N. Waring, A. Dey, K. Ozato, B. Lai, W. Peng, and K. Ge. 2017. Brd4 binds to active enhancers to control cell identity gene induction in adipogenesis and myogenesis. *Nat. Commun.* 8:2217. https://doi.org/10.1038/s41467-017-02403-5

Liu, Z., Y. Guo, S. Tang, L. Zhou, C. Huang, Y. Cao, H. Huang, X. Wu, D. Meng, L. Ye, et al. 2019. Cutting Edge: Transcription Factor BCL6 Is Required for the Generation, but Not Maintenance, of Memory CD8$^+$ T Cells in Acute Viral Infection. *J. Immunol.* 203:323–327. https://doi.org/10.4049/jimmunol.1900014

Lovén, J., H.A. Hoke, C.Y. Lin, A. Lau, D.A. Orlando, C.R. Vakoc, J.E. Bradner, T.I. Lee, and R.A. Young. 2013. Selective inhibition of tumor oncogenes by disruption of super-enhancers. *Cell.* 153:320–334. https://doi.org/10.1016/j.cell.2013.03.036

Mackay, L.K., A. Rahimpour, J.Z. Ma, N. Collins, A.T. Stock, M.-L. Hafon, J. Vega-Ramos, P. Lauzurica, S.N. Mueller, T. Stefanovic, et al. 2013. The developmental pathway for CD103(+)CD8+ tissue-resident memory T cells of skin. *Nat. Immunol.* 14:1294–1301. https://doi.org/10.1038/ni.2744

Mao, W., A. Ghasemzadeh, Z.T. Freeman, A. Obradovic, M.G. Chaimowitz, T.R. Nirschl, E. McKiernan, S. Yegnasubramanian, and C.G. Drake. 2019. Immunogenicity of prostate cancer is augmented by BET bromodomain inhibition. *J. Immunother. Cancer.* 7:277. https://doi.org/10.1186/s40425-019-0758-y

Masson, F., M. Minnich, M. Olshansky, I. Bilic, A.M. Mount, A. Kallies, T.P. Speed, M. Busslinger, S.L. Nutt, and G.T. Belz. 2013. Id2-mediated inhibition of E2A represses memory CD8+ T cell differentiation. *J. Immunol.* 190:4585–4594. https://doi.org/10.4049/jimmunol.1300099

Mele, D.A., A. Salmeron, S. Ghosh, H.-R. Huang, B.M. Bryant, and J.M. Lora. 2013. BET bromodomain inhibition suppresses TH17-mediated pathology. *J. Exp. Med.* 210:2181–2190. https://doi.org/10.1084/jem.20130376

Miller, B.C., D.R. Sen, R. Al Abosy, K. Bi, Y.V. Virkud, M.W. LaFleur, K.B. Yates, A. Lako, K. Felt, G.S. Naik, et al. 2019. Subsets of exhausted CD8$^+$ T cells differentially mediate tumor control and respond to checkpoint blockade. *Nat. Immunol.* 20:326–336. https://doi.org/10.1038/s41590-019-0312-6

Milner, J.J., and A.W. Goldrath. 2018. Transcriptional programming of tissue-resident memory CD8$^+$ T cells. *Curr. Opin. Immunol.* 51:162–169. https://doi.org/10.1016/j.coi.2018.03.017

Milner, J.J., C. Toma, B. Yu, K. Zhang, K. Omilusik, A.T. Phan, D. Wang, A.J. Getzler, T. Nguyen, S. Crotty, et al. 2017. Runx3 programs CD8$^+$ T cell residency in non-lymphoid tissues and tumours. *Nature.* 552:253–257. https://doi.org/10.1038/nature24993

Milner, J.J., H. Nguyen, K. Omilusik, M. Reina-Campos, M. Tsai, C. Toma, A. Delpoux, B.S. Boland, S.M. Hedrick, J.T. Chang, and A.W. Goldrath. 2020a. Delineation of a molecularly distinct terminally differentiated memory CD8 T cell population. *Proc. Natl. Acad. Sci. USA.* 117:25667–25678. https://doi.org/10.1073/pnas.2008571117

Milner, J.J., C. Toma, Z. He, N.S. Kurd, Q.P. Nguyen, B. McDonald, L. Quezada, C.E. Widjaja, D.A. Witherden, J.T. Crowl, et al. 2020b. Heterogenous Populations of Tissue-Resident CD8$^+$ T Cells Are Generated in Response

to Infection and Malignancy. *Immunity.* 52:808–824.e7. https://doi.org/10.1016/j.immuni.2020.04.007

Mollo, S.B., J.T. Ingram, R.L. Kress, A.J. Zajac, and L.E. Harrington. 2014. Virus-specific CD4 and CD8 T cell responses in the absence of Th1-associated transcription factors. *J. Leukoc. Biol.* 95:705–713. https://doi.org/10.1189/jlb.0813429

Olson, J.A., C. McDonald-Hyman, S.C. Jameson, and S.E. Hamilton. 2013. Effector-like CD8$^+$ T cells in the memory population mediate potent protective immunity. *Immunity.* 38:1250–1260. https://doi.org/10.1016/j.immuni.2013.05.009

Omilusik, K.D., J.A. Best, B. Yu, S. Goossens, A. Weidemann, J.V. Nguyen, E. Seuntjens, A. Stryjewska, C. Zweier, R. Roychoudhuri, et al. 2015. Transcriptional repressor ZEB2 promotes terminal differentiation of CD8+ effector and memory T cell populations during infection. *J. Exp. Med.* 212:2027–2039. https://doi.org/10.1084/jem.20150194

Omilusik, K.D., M.S. Nadjsombati, L.A. Shaw, B. Yu, J.J. Milner, and A.W. Goldrath. 2018. Sustained Id2 regulation of E proteins is required for terminal differentiation of effector CD8$^+$ T cells. *J. Exp. Med.* 215:773–783. https://doi.org/10.1084/jem.20171584

Ott, C.J., N. Kopp, L. Bird, R.M. Paranal, J. Qi, T. Bowman, S.J. Rodig, A.L. Kung, J.E. Bradner, and D.M. Weinstock. 2012. BET bromodomain inhibition targets both c-Myc and IL7R in high-risk acute lymphoblastic leukemia. *Blood.* 120:2843–2852. https://doi.org/10.1182/blood-2012-02-413021

Pauken, K.E., M.A. Sammons, P.M. Odorizzi, S. Manne, J. Godec, O. Khan, A.M. Drake, Z. Chen, D.R. Sen, M. Kurachi, et al. 2016. Epigenetic stability of exhausted T cells limits durability of reinvigoration by PD-1 blockade. *Science.* 354:1160–1165. https://doi.org/10.1126/science.aaf2807

Philip, M., L. Fairchild, L. Sun, E.L. Horste, S. Camara, M. Shakiba, A.C. Scott, A. Viale, P. Lauer, T. Merghoub, et al. 2017. Chromatin states define tumour-specific T cell dysfunction and reprogramming. *Nature.* 545:452–456. https://doi.org/10.1038/nature22367

Preston, G.C., C. Feijoo-Carnero, N. Schurch, V.H. Cowling, and D.A. Cantrell. 2013. The impact of KLF2 modulation on the transcriptional program and function of CD8 T cells. *PLoS One.* 8:e77537. https://doi.org/10.1371/journal.pone.0077537

Ren, C., G. Zhang, F. Han, S. Fu, Y. Cao, F. Zhang, Q. Zhang, J. Meslamani, Y. Xu, D. Ji, et al. 2018. Spatially constrained tandem bromodomain inhibition bolsters sustained repression of BRD4 transcriptional activity for TNBC cell growth. *Proc. Natl. Acad. Sci. USA.* 115:7949–7954. https://doi.org/10.1073/pnas.1720000115

Rutishauser, R.L., G.A. Martins, S. Kalachikov, A. Chandele, I.A. Parish, E. Meffre, J. Jacob, K. Calame, and S.M. Kaech. 2009. Transcriptional repressor Blimp-1 promotes CD8(+) T cell terminal differentiation and represses the acquisition of central memory T cell properties. *Immunity.* 31:296–308. https://doi.org/10.1016/j.immuni.2009.05.014

Shi, J., and C.R. Vakoc. 2014. The mechanisms behind the therapeutic activity of BET bromodomain inhibition. *Mol. Cell.* 54:728–736. https://doi.org/10.1016/j.molcel.2014.05.016

Shu, S., C.Y. Lin, H.H. He, R.M. Witwicki, D.P. Tabassum, J.M. Roberts, M. Janiszewska, S.J. Huh, Y. Liang, J. Ryan, et al. 2016. Response and resistance to BET bromodomain inhibitors in triple-negative breast cancer. *Nature.* 529:413–417. https://doi.org/10.1038/nature16508

Siddiqui, I., K. Schaeuble, V. Chennupati, S.A. Fuertes Marraco, S. Calderon-Copete, D. Pais Ferreira, S.J. Carmona, L. Scarpellino, D. Gfeller, S. Pradervand, et al. 2019. Intratumoral Tcf1$^+$PD-1$^+$CD8$^+$ T Cells with Stem-like Properties Promote Tumor Control in Response to Vaccination and Checkpoint Blockade Immunotherapy. *Immunity.* 50:195–211.e10. https://doi.org/10.1016/j.immuni.2018.12.021

Utzschneider, D.T., A. Delpoux, D. Wieland, X. Huang, C.Y. Lai, M. Hofmann, R. Thimme, and S.M. Hedrick. 2018. Active Maintenance of T Cell Memory in Acute and Chronic Viral Infection Depends on Continuous Expression of FOXO1. *Cell Rep.* 22:3454–3467. https://doi.org/10.1016/j.celrep.2018.03.020

Wang, D., H. Diao, A.J. Getzler, W. Rogal, M.A. Frederick, J. Milner, B. Yu, S. Crotty, A.W. Goldrath, and M.E. Pipkin. 2018. The Transcription Factor Runx3 Establishes Chromatin Accessibility of cis-Regulatory Landscapes that Drive Memory Cytotoxic T Lymphocyte Formation. *Immunity.* 48:659–674.e6. https://doi.org/10.1016/j.immuni.2018.03.028

Whyte, W.A., D.A. Orlando, D. Hnisz, B.J. Abraham, C.Y. Lin, M.H. Kagey, P.B. Rahl, T.I. Lee, and R.A. Young. 2013. Master transcription factors and mediator establish super-enhancers at key cell identity genes. *Cell.* 153(2):307–319. https://doi.org/10.1016/j.cell.2013.03.035

Wu, S.-Y., A.-Y. Lee, H.-T. Lai, H. Zhang, and C.-M. Chiang. 2013. Phospho switch triggers Brd4 chromatin binding and activator recruitment for gene-specific targeting. *Mol. Cell.* 49:843–857. https://doi.org/10.1016/j.molcel.2012.12.006

Yang, Z., J.H. Yik, R. Chen, N. He, M.K. Jang, K. Ozato, and Q. Zhou. 2005. Recruitment of P-TEFb for stimulation of transcriptional elongation by the bromodomain protein Brd4. *Mol. Cell.* 19:535–545. https://doi.org/10.1016/j.molcel.2005.06.029

Yang, C.Y., J.A. Best, J. Knell, E. Yang, A.D. Sheridan, A.K. Jesionek, H.S. Li, R.R. Rivera, K.C. Lind, L.M. D'Cruz, et al. 2011. The transcriptional regulators Id2 and Id3 control the formation of distinct memory CD8+ T cell subsets. *Nat. Immunol.* 12:1221–1229. https://doi.org/10.1038/ni.2158

Yu, B., K. Zhang, J.J. Milner, C. Toma, R. Chen, J.P. Scott-Browne, R.M. Pereira, S. Crotty, J.T. Chang, M.E. Pipkin, et al. 2017. Epigenetic landscapes reveal transcription factors that regulate CD8$^+$ T cell differentiation. *Nat. Immunol.* 18:573–582. https://doi.org/10.1038/ni.3706

Zhou, X., S. Yu, D.M. Zhao, J.T. Harty, V.P. Badovinac, and H.H. Xue. 2010. Differentiation and persistence of memory CD8(+) T cells depend on T cell factor 1. *Immunity.* 33:229–240. https://doi.org/10.1016/j.immuni.2010.08.002

Zhu, H., F. Bengsch, N. Svoronos, M.R. Rutkowski, B.G. Bitler, M.J. Allegrezza, Y. Yokoyama, A.V. Kossenkov, J.E. Bradner, J.R. Conejo-Garcia, and R. Zhang. 2016. BET bromodomain inhibition promotes anti-tumor immunity by suppressing PD-L1 expression. *Cell Rep.* 16:2829–2837. https://doi.org/10.1016/j.celrep.2016.08.032

Supplemental material

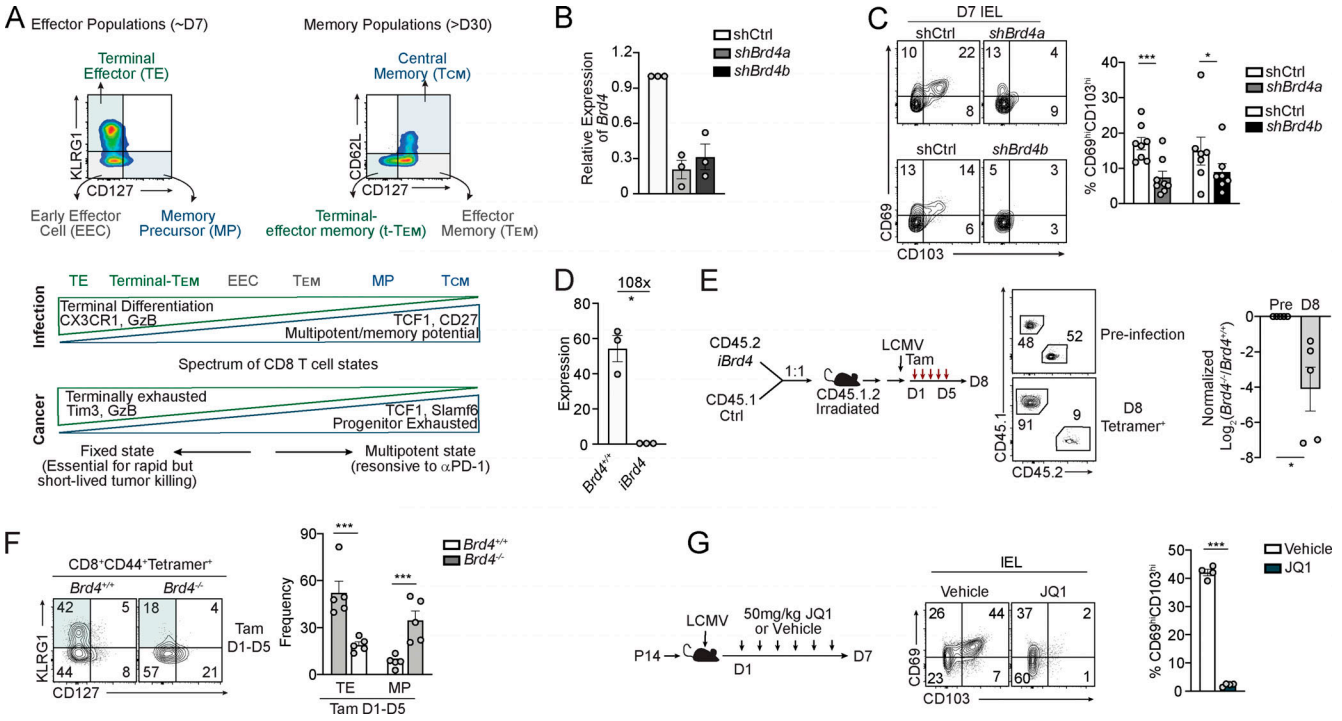

Figure S1. **BRD4 regulates CD8 T cell differentiation during infection. (A)** Model of effector and memory T cell populations during infection and their corresponding characteristics (top). Spectrum of CD8 T cell states during infection and cancer (bottom). **(B)** Gene expression analysis of *Brd4* in sorted CD8 T cells transduced with *shBrd4*- or shCtrl-encoding retroviruses after in vitro culturing for 4–5 d. **(C)** Congenically distinct P14 cells were transduced with *Brd4* shRNA–encoding or control shRNA–encoding retroviruses and transferred into recipient mice that were subsequently infected with LCMV. The frequency of CD103- and CD69-expressing P14 cells in the epithelium of the small intestine on day 7 of infection was evaluated. **(D)** RNA sequencing expression levels of the floxed *Brd4* region based on the experimental schematic in Fig. 3 A. **(E)** Bone marrow chimera mice were generated by adoptive transfer of 1:1 mixed bone marrow cells from CD45.1 $Brd4^{+/+}$ control mice (Ctrl) and CD45.2 $Brd4^{fl/fl}Ert2^{Cre/+}$ mice (inducible *Brd4* [*iBrd4*]) into irradiated mice (left). Reconstituted mice were infected with LCMV and treated with tamoxifen on days 1–5 of infection to induce deletion of *Brd4*. Representative flow cytometry plots (right) and quantification (bottom left) of the ratio of $Brd4^{fl/fl}Ert2^{Cre/+}$ and control cells before infection and 8 d after infection. **(F)** Frequency of CD127- and KLRG1-expressing tetramer+ cells from D. **(G)** Naive P14 CD8 T cells were transferred into congenically distinct recipient mice that were subsequently infected with LCMV. Infected mice were treated daily with 50 mg/kg JQ1 or vehicle (left). Frequency of CD103- and CD69-expressing P14 cells in the epithelium of the small intestine on day 7 of infection (right). Graphs show mean ± SEM of *n* = 5–8 mice pooled from two independent experiments (C–E); *n* = 4 from one representative of two independent experiments (F); or data pooled from three independent experiments (B). *, P < 0.05; ***, P < 0.005. Symbols represent an individual mouse (C–F). IEL, intraepithelial lymphocyte.

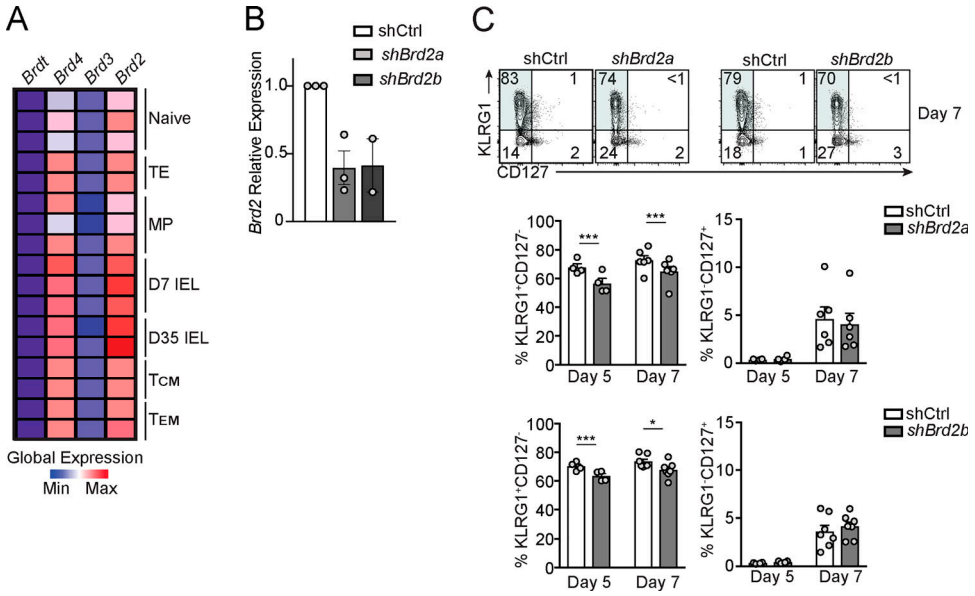

Figure S2. **Impact of *Brd2* knockdown on CD8 T cell differentiation during infection. (A)** Global relative expression of BET family members among naive, effector (D7), and memory populations (D35) from Milner et al. (2017). **(B)** Gene expression analysis of *Brd2* in sorted CD8 T cells transduced with *shBrd2*- or shCtrl-encoding retroviruses. **(C)** Congenically distinct P14 cells were transduced with *Brd2* shRNA–encoding or control shRNA–encoding retroviruses. Transduced cells were transferred into recipient mice that were subsequently infected with LCMV, and the phenotype of donor cells was evaluated on day 7 of infection. *, P < 0.05; ***, P < 0.005. IEL, intraepithelial lymphocyte.

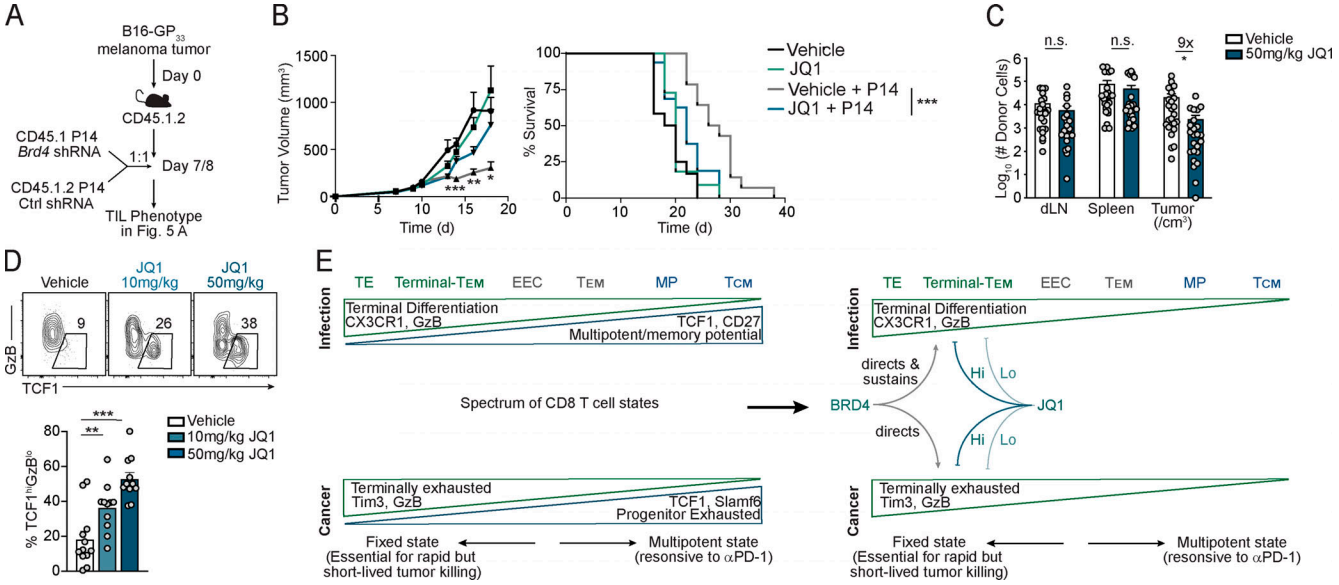

Figure S3. **JQ1 treatment impairs adoptive cell therapy efficacy in an immunocompetent mouse model. (A)** Model for Fig 5 A, wherein congenically distinct P14 cells were transduced with two distinct *Brd4* shRNA–encoding or control shRNA–encoding retroviruses. Transduced cells were then mixed 1:1 and transferred into mice bearing established B16-GP$_{33-41}$ tumors. **(B)** Tumor growth and mortality from experiment in Fig. 5 D. **(C)** P14 cells were enumerated in the tumor, tumor draining lymph node (dLN), and spleen 8–12 d after adoptive transfer with daily treatment of 50 mg/kg JQ1 or vehicle. **(D)** Frequency of TCF1^{hi}GzB^{lo} P14 cells after daily in vivo treatment of 50 mg/kg JQ1, 10 mg/kg JQ1, or vehicle in tumor-bearing mice. **(E)** Model of CD8 T cell states during infection and cancer (left) and summary of the role of BRD4 and JQ1 treatment in the regulation of CD8 T cell differentiation (right). Graphs show mean ± SEM of *n* = 11–16 mice pooled from two independent experiments (B); *n* = 11–12 mice pooled from three independent experiments (D); or *n* = 22–24 pooled from six independent experiments (C). *, P < 0.05; **, P < 0.01; ***, P < 0.005. Symbols represent an individual mouse (C and D).

Table S1 is provided online and shows summary Z-scores from in vivo RNAi screening approach.